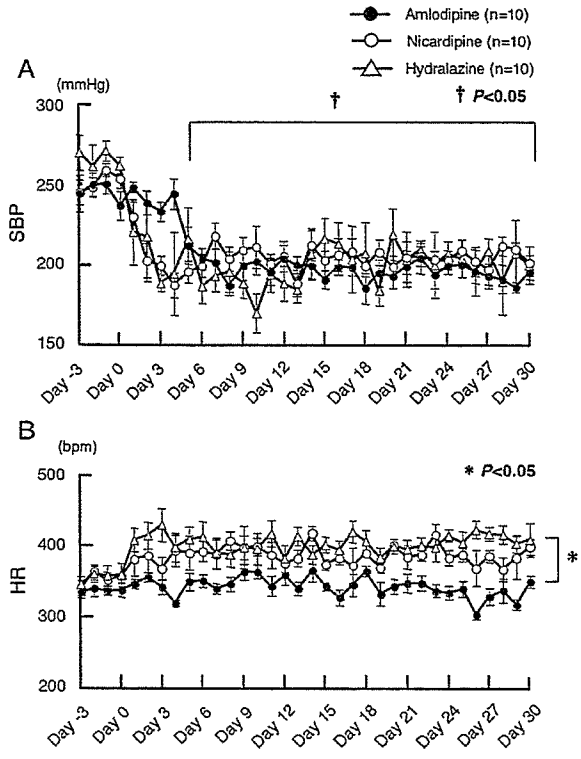

Fig. 1. *Time course of changes in systolic blood pressure (SBP) (A) and heart rate (HR) (B) induced by treatment with amlodipine, nicardipine and hydralazine.* †$p < 0.05$ *compared with the baseline values.* *$p < 0.05$ *for the difference between the two groups.*

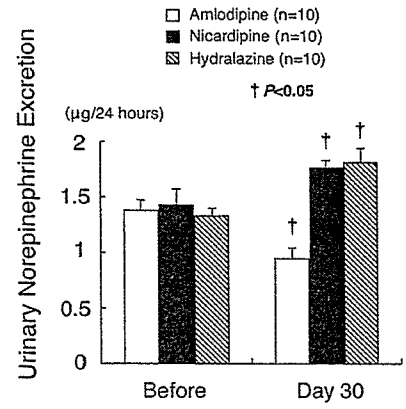

Fig. 2. *Urinary norepinephrine excretion for 24 h before and during the last day of (after) treatment with amlodipine, nicardipine and hydralazine.* †$p < 0.05$ *compared with the values before treatment.*

with coronary artery disease, which is probably due to arterial baroreflex-mediated sympathoexcitation, particularly when short-acting calcium channel blockers are used (*3–5*). However, recent large clinical trials have indicated that this is not necessarily the case with long-acting dihydropyridine calcium channel blockers, such as amlodipine (*1, 2*). In addition, amlodipine has been demonstrated to have anti-atherosclerotic and anti-inflammatory effects in animals (*6–9*) and humans (*10*). The mechanisms involved are complex, and include an increase in nitric oxide production (*11*) and a decrease in oxidative stress (*12–14*).

The reported effects of amlodipine on sympathetic nerve activity vary among human studies, although it appears to lower blood pressure (*15–17*). Receptor binding sites for calcium channel blockers have been identified in the brain (*18–20*). In conscious spontaneously hypertensive rats (SHR), intracerebroventricular administration of nifedipine or amlodipine decreases blood pressure, heart rate and renal sympathetic nerve activity (*21, 22*). Furthermore, long-term i.v. infusion of nifedipine or amlodipine decreases these variables by inhibiting central sympathetic outflow (*21, 22*).

Increased nitric oxide levels and decreased oxidative stress in the brain, particularly in the brainstem, inhibit sympathetic nerve activity, thereby reducing blood pressure in stroke-prone SHR (SHRSP) (*23*). Increased oxidative stress is also involved in the pathogenesis of hypertension and hypertensive vascular lesion formation (*24*). We demonstrated previously that oxidative stress in the brain is increased in SHRSP, which is related to the increased sympathetic outflow in this model (*23*). Amlodipine reduces oxidative stress in the vasculature of hypertensive animals (*25*) and humans (*26, 27*). However, the antioxidant effect of amlodipine in the brain of hypertensive animals has not been reported previously. Therefore, the aim of the present study was to determine whether long-term oral treatment with amlodipine reduced oxidative stress in the brain of SHRSP, and to examine the associated changes in blood pressure, heart rate, and urinary norepinephrine excretion. For this purpose, we measured thiobarbituric acid-reactive substances (TBARS), which are the end products of lipid peroxidation and markers of oxidative stress (*23*). Electron spin resonance spectroscopy measurements (*23*) were also performed to analyze the production of reactive oxygen species.

Methods

General Preparation

This study was reviewed and approved by the Committee of Ethics of Animal Experiments, Kyushu University Graduate School of Medical Sciences, Japan. Male SHRSP/Izm (*14* weeks old; SLC Japan, Hamamatsu, Japan) were fed a standard diet with free access to drinking water. The animals received amlodipine in their drinking water at doses (3 or 10 mg/kg body weight/day) that were chosen based on previous studies (*12, 28–30*). Control groups were fed a standard diet

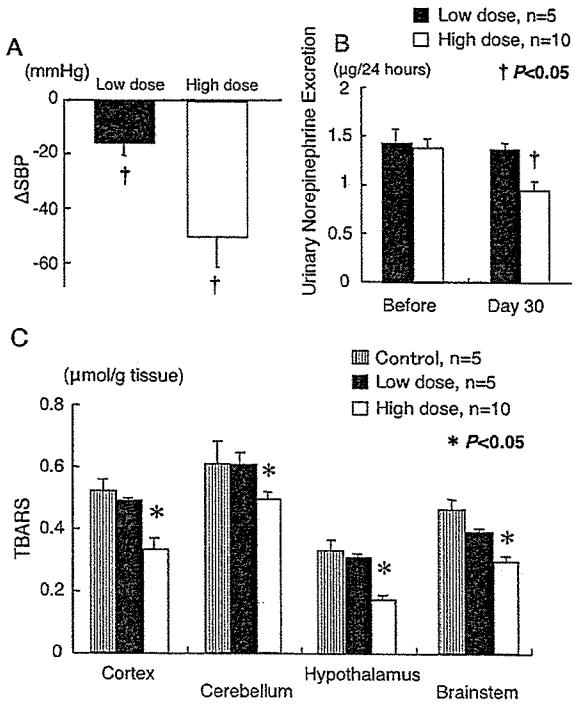

Fig. 3. *A: Amlodipine-induced changes in systolic blood pressure (ΔSBP) at doses of 3 or 10 mg/kg body weight/day. B: Urinary norepinephrine excretion for 24 h before and after amlodipine treatment. C: Levels of TBARS in the brain (cortex, cerebellum, hypothalamus and brainstem) in non-treated rats (control) and rats treated with amlodipine.* $^{\dagger}p < 0.05$ *compared with the baseline values.* $^{*}p < 0.05$ *for the difference between the two groups.*

and received nicardipine (10 mg/kg body weight/day) or hydralazine (20 mg/kg body weight/day) in their drinking water. The treatment commenced when the rats were 14 weeks of age and continued for 30 days. All drugs were dissolved in 45 ml of drinking water per day and, once this had been consumed, additional water was made available *ad libitum*.

Measurement of Blood Pressure, Heart Rate, and Urinary Norepinephrine Excretion

Systolic blood pressure and heart rate evaluated using the tail-cuff method were measured before and after treatment with amlodipine and the other drugs in SHRSP, as described previously (*31*). Urine was collected for 24 h in a metabolic cage. Urinary norepinephrine concentrations were measured before and after amlodipine, nicardipine or hydralazine treatment using high-performance liquid chromatography. Urinary norepinephrine excretion was calculated as a marker of sympathetic nerve activity (*23*, *31*).

Measurement of TBARS

Brain tissue was homogenized in 1.15% KCl (pH 7.4), and 0.4% sodium dodecyl sulfate, 7.5% acetic acid adjusted to pH 3.5 with NaOH and 0.3% TBA were added to the homogenate. The amounts of TBARS were determined by absorbance with a molecular extinction coefficient of 156,000 and expressed as μmol/g of wet weight tissue, as described previously (*23*, *32*).

Electron Spin Resonance Spectroscopy Measurements

Electron spin resonance spectroscopy measurements were performed at room temperature with an X-band (9.45-GHz) electron spin resonance spectrometer (JES-RE-1X; JEOL, Tokyo, Japan) at the following settings: microwave power of 10 mW, an external magnetic field range of 20 mT and a scan rate of 10 mT/min. The amounts of reactive oxygen species were quantified by monitoring the time-dependent decay of the amplitude of the electron spin resonance spectra elicited by the nitroxide radical 4-hydroxy-2,2,6,6-tetramethyl-piperidine-*N*-oxyl (hydroxy-TEMPO) as a spin probe. The tissue was homogenized in 50 mmol/l phosphate-buffered saline (PBS) containing the following protease inhibitors: leupeptin (10 g/ml), phenylmethylsulfonyl fluoride (100 g/ml), dithiothreitol (1 mmol/l) and trypsin inhibitor (10 μg/ml). The homogenate was mixed rapidly with hydroxy-TEMPO (0.1 mmol/l) in PBS and drawn into glass tubes. The electron spin resonance spectra were recorded for up to 10 min at 10-s intervals, as described previously (*23*, *32*, *33*).

Continuous Intracisternal (i.c.) Infusion Experiments with Amlodipine

The SHRSP were randomly divided into two groups, which received either artificial cerebrospinal fluid vehicle (n=5) or amlodipine (dissolved in artificial cerebrospinal fluid; 0.1 mg/kg body weight/day; n=6) by continuous i.c. infusion (0.25 μl/h) for 2 weeks *via* an osmotic minipump (Alzet model 1002; DURECT Corp., Cupertino, USA), as described previously (*34*, *35*). The treatment commenced when the rats were 14 weeks of age and continued for 2 weeks. Systolic blood pressure, heart rate, urinary norepinephrine concentrations, and levels of TBARS were measured before and after the infusion.

Drugs

Amlodipine was provided from Pfizer Japan Inc. Other drugs were purchased from Sigma Chemical Co. (St. Louis, USA).

Statistical Analysis

All values are expressed as the mean±SEM). Two-way anal-

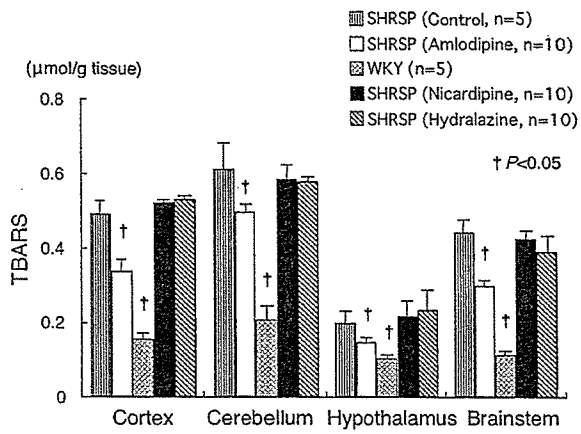

Fig. 4. *Levels of TBARS in the brain (cortex, cerebellum, hypothalamus and brainstem) in non-treated rats (control) and rats treated with amlodipine, nicardipine or hydralazine.* †p < *0.05 compared with the values for non-treated rats.*

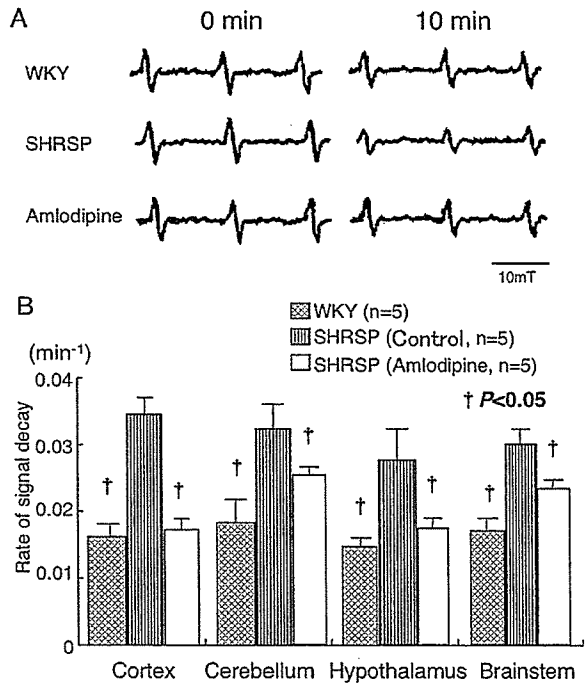

Fig. 5. *Electron spin resonance analysis of hydroxy-TEMPO in the tissues. A: Sequential sample of electron spin resonance spectra of hydroxy-TEMPO in brainstem tissues from SHRSP (middle spectra), SHRSP treated with amlodipine (lower spectra) and WKY rats (upper spectra). B: Summary data for the signal decay rate in the brain (cortex, cerebellum, hypothalamus and brainstem) in WKY rats, SHRSP and SHRSP treated with amlodipine.* †p < *0.05 compared with the values for non-treated SHRSP (control).*

ysis of variance (ANOVA) was used to compare the systolic blood pressure and heart rate between the amlodipine-treated and other groups. Comparisons between any two mean values were performed using Bonferroni's correction for multiple comparisons. ANOVA was used to compare the amounts of TBARS and the electron spin resonance signal-decay rates in non-treated SHRSP and other rats in conjunction with a *post hoc* test using Scheffe's correction. A paired *t*-test was performed to compare the urinary norepinephrine excretion before and after treatment. Differences were considered to be statistically significant when p was less than 0.05.

Results

Effects of Amlodipine on Blood Pressure, Heart Rate, and Urinary Norepinephrine Excretion

Systolic blood pressure was reduced to similar levels in the high-dose amlodipine- and hydralazine-treated groups; the values for amlodipine, nicardipine and hydralazine were -40 ± 12, -45 ± 7 and -43 ± 8 mmHg, respectively ($n=10$ for each; Fig. 1A). By contrast, heart rate was not significantly affected by amlodipine treatment, but was increased by nicardipine and hydralazine treatment (Fig. 1B). Urinary norepinephrine excretion was significantly higher in SHRSP than in WKY rats, with values of 1.38 ± 0.10 and 0.76 ± 0.03 μg/day, respectively ($n=6$ for both; $p<0.05$). Furthermore, urinary norepinephrine excretion was decreased in SHRSP after amlodipine treatment, but was significantly increased after nicardipine or hydralazine treatment; the values were 1.37 ± 0.15 *vs.* 0.87 ± 0.10 μg/day, 1.45 ± 0.17 *vs.* 1.68 ± 0.06 μg/day and 1.33 ± 0.08 *vs.* 1.77 ± 0.14 μg/day for amlodipine, nicardipine, and hydralazine, respectively ($n=10$; $p<0.05$; Fig. 2). Treatment with a high dose of amlodipine decreased the systolic blood pressure to a greater extent than treatment with a low dose, with values of -40 ± 12 and -18 ± 7 mmHg, respectively ($p<0.05$; Fig. 3A). Urinary norepinephrine excretion was not significantly different before and after treatment with a low dose of amlodipine (1.44 ± 0.25 *vs.* 1.38 ± 0.15 μg/day; Fig. 3B).

Reactive Oxygen Species Generation in the Brain

Levels of TBARS in the cortex, cerebellum, hypothalamus and brainstem were significantly higher in SHRSP than in WKY rats ($p<0.05$; $n=5$ for both). Furthermore, levels of TBARS in each area of the brain examined were significantly reduced in the high-dose amlodipine-treated, but not in the nicardipine- or hydralazine-treated, SHRSP ($p<0.05$; $n=10$ for each; Fig. 4). The levels of TBARS in all areas of the brain examined were not significantly altered in the low-dose amlodipine-treated SHRSP (Fig. 3C). The intensity of electron spin resonance signals in each area of the brain decreased more rapidly in SHRSP than in WKY rats (Fig. 5A). The rates

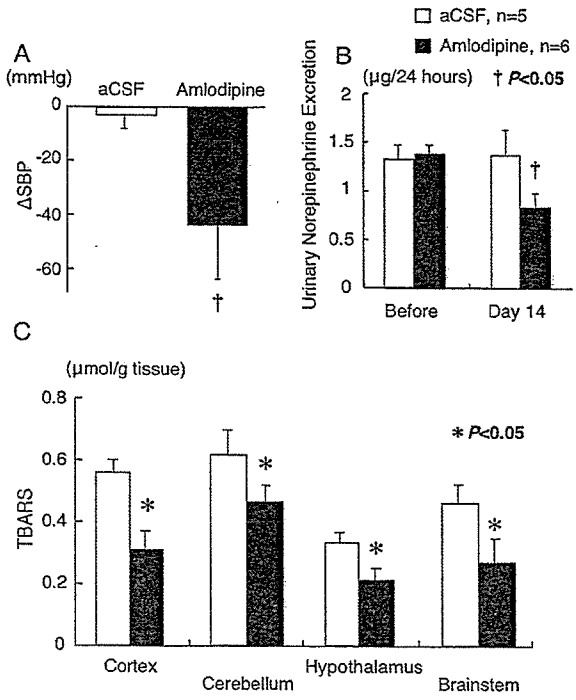

Fig. 6. *A: Changes in systolic blood pressure (ΔSBP) caused by continuous i.c. infusion with amlodipine or artificial cerebrospinal fluid (aCSF) for 2 weeks. B: Urinary norepinephrine excretion for 24 h at days 0 and 14. C: Levels of TBARS in the brain (cortex, cerebellum, hypothalamus and brainstem) in non-treated rats and rats treated with amlodipine at days 0 and 14.* †p < *0.05 compared with the values before treatment.* *p < *0.05 for the difference between the two groups.*

of signal decay in the cortex, cerebellum, hypothalamus and brainstem, calculated from the slopes of the lines, were significantly higher in SHRSP than in WKY rats ($p<0.05$; $n=5$ for each; Fig. 5B). Furthermore, the rates of signal decay in these areas of the brain were significantly reduced in amlodipine-treated SHRSP ($p<0.05$; $n=5$ for each; Fig. 5B).

Effect of Continuous i.c. Infusion with Amlodipine

The changes in systolic blood pressure after the i.c. infusion of amlodipine for 2 weeks are shown in Fig. 6A. The changes in systolic blood pressure were significantly greater after treatment with amlodipine (−43±22 mmHg; $n=6$) than after treatment with artificial cerebrospinal fluid (−3±12 mmHg; $n=5$; $p<0.05$). Figure 6B shows that urinary norepinephrine excretion was significantly decreased in SHRSP after treatment with amlodipine (1.45±0.10 *vs.* 0.67±0.11; $n=6$; $p<0.05$), but was not significantly altered by treatment with artificial cerebrospinal fluid (1.42±0.08 *vs.* 1.48±0.20 μg/day; $n=5$). The levels of TBARS in all areas of the brain were significantly reduced in amlodipine- but not artificial cerebrospinal fluid-treated SHRSP ($n=6$ and 5, respectively; $p<0.05$; Fig. 6C).

Discussion

The major findings of the present study were that oral treatment with amlodipine did not induce reflex tachycardia and reduced sympathetic nerve activity. In addition, amlodipine decreased oxidative stress in the brains of SHRSP, as evaluated by the measurement of levels of TBARS. By contrast, treatment with hydralazine induced sympathoexcitation and reflex tachycardia, but did not alter levels of TBARS. Nicardipine, which is another calcium channel blocker, also induced sympathoexcitation and reflex tachycardia, but did not alter TBARS levels. The electron spin resonance spectroscopy results indicated increased reactive oxygen species production in SHRSP, which was attenuated after treatment with amlodipine. These findings suggest that long-term antihypertensive treatment with amlodipine does not cause reflex-induced sympathoexcitation and reduces the increased oxidative stress in the brains of SHRSP. In particular, the decreased oxidative stress levels in the brainstem and hypothalamus might be related to a decrease in sympathetic nerve activity.

A gradual decrease in blood pressure was observed over time in rats treated with amlodipine compared with those treated with hydralazine or nicardipine, due to differences in the pharmacokinetic profiles, plasma concentrations and lipophilicities of the drugs (*16*, *21–33*, *36*). Disrupted tight junctions caused by endothelial dysfunction are responsible for the increased permeability of tracers through the blood–brain barrier in chronic hypertension (*37*). L-type voltage-gated calcium channels in the central nervous system and dihydropyridines act on these receptors (*19*, *20*, *38–40*). Thus, it is possible that lipophilic dihydropyridines (such as nifedipine and amlodipine) are able to cross the blood–brain barrier in chronic hypertension (*21*, *22*) and reduce the generation of reactive oxygen species (*41–43*). However, this might not occur with all calcium channel blockers, as nicardipine did not reduce the generation of reactive oxygen species.

We believe that treatment with the lower dose of amlodipine in our study was not sufficient to reduce the oxidative stress in the brain. In addition, urinary norepinephrine excretion was not altered. By contrast, treatment with the higher dose of amlodipine induced a greater reduction in blood pressure, which was associated with a decrease in urinary norepinephrine excretion. Oxidative stress in the brain was also reduced. A greater reduction in blood pressure is thought to elicit a greater reflex increase in sympathetic nerve activity. Thus, these results suggest that treatment with amlodipine, at a dose that is sufficient to decrease blood pressure, reduces oxidative stress in the brain in association with sympathoinhibition.

Brain cell membranes contain a high concentration of polyunsaturated fatty acids (*44*). These are targets of free radicals, which cause chain reactions of lipid peroxidation (*45*). TBARS, which are the end products of lipid peroxidation and markers of oxidative stress, were increased in the brain of SHRSP (*23*). In the present study, we examined levels of TBARS in the cortex, cerebellum, hypothalamus and brainstem, and found that they were all increased in SHRSP compared with WKY rats. This was consistent with the results of our recent study, in which we compared levels of TBARS in the whole brain, the rostral ventrolateral medulla and the nucleus tractus solitarius of SHRSP and WKY rats (*46*). These areas are important for autonomic cardiovascular regulation (*47*, *48*). The electron spin resonance spectroscopy results further support the theory that there is increased generation of reactive oxygen species in the brain of SHRSP compared with WKY rats. Moreover, this increase was attenuated by amlodipine.

Although variable effects on the sympathetic nervous system have been reported in clinical studies in humans (*16–18*, *26*), lipophilic dihydropyridines (such as nifedipine and amlodipine) are believed to have sympatho-inhibitory and depressor effects through central nervous system mechanisms in SHR (*21*, *22*). During long-term i.v. infusion, nifedipine and amlodipine cross the blood–brain barrier and, thereafter, inhibit sympathetic nerve activity and reduce blood pressure (*21*, *22*). Furthermore, intracerebroventricular injection of these calcium channel blockers reduces blood pressure, heart rate, and renal sympathetic nerve activity (*21*, *22*). In addition, direct microinjection of calcium channel blockers into the nucleus tractus solitarius of the brainstem reduces blood pressure and heart rate *via* the inhibition of central sympathetic outflow (*49*). In the present study, amlodipine administered by i.c. infusion decreased blood pressure, urinary norepinephrine excretion and oxidative stress in the brain, further supporting the idea that it elicits these effects by acting on the central nervous system. There were no effects on blood pressure and heart rate when we intravenously administered the same concentration of amlodipine as used for the intracisternal infusion for 1 h (data not shown). Although the site of the sympatho-inhibitory actions of amlodipine in the central nervous system is not known, we consider the hypothalamus and brainstem to be likely candidates. In conjunction with the decrease in reactive oxygen species generation, an increase in endothelial nitric oxide synthase activity might be related to the decrease in oxidative stress and central sympathetic outflow in SHRSP (*31*, *50–52*). In fact, amlodipine enhances endothelial nitric oxide synthase activity (*53*), although we did not address this issue in the present study. Increased nitric oxide production in the brainstem also produces a decrease in central sympathetic outflow (*50–52*). Amlodipine may reduce reactive oxygen species by upregulating Cu/Zn superoxide dismutase in SHRSP (*54*).

Several previous studies have suggested that the generation of reactive oxygen species leads to hypertensive vascular-lesion formation (*55–60*). Therefore, therapies aimed at reducing the generation of reactive oxygen species might be useful for hypertensive patients. In particular, the brain is the organ that is most affected by hypertension (*55*). In the present study, we demonstrated that oral treatment with amlodipine reduced oxidative stress in the cortex and cerebellum, as well as the hypothalamus and brainstem; the effects on the latter might help reduce sympathetic nerve activity, thereby preventing cardiovascular events, whereas the effects on the former might help to protect brain function. Hypertension accelerates age-related organ damage, which is also associated with sympathetic dysregulation (*55*, *56*). In addition, dementia might be related to hypertension (*60*). Further studies will be required to examine how treatment with amlodipine leads to the reduction of reactive oxygen species. It is possible that long-term treatment for hypertension, as well as the reduction of oxidative stress in the brain, will result in a better quality of life for patients.

We cannot exclude the possibility that amlodipine might act on the peripheral sympathetic nervous system, thereby inhibiting the sympathetic nerve activity. In particular, amlodipine has been shown to block both N-type Ca^{2+} channels and L-type Ca^{2-} channels (*61*, *62*), although the extent of these actions has not been clarified *in vivo*. Nicardipine has also been reported to exhibit this blocking activity (*62*). However, we found different results between amlodipine and nicardipine. Furthermore, the present study does not provide direct evidence that an increase in oxidative stress in the brain inhibits sympathetic nerve activity, thereby reducing blood pressure. Thus, it remains unknown whether the decrease in reactive oxygen species in the brain is a cause or an effect of sympatho-inhibition or blood pressure reduction from the results of the present study. The reduction of blood pressure itself, however, did not decrease oxidative stress in the brain when we administered hydralazine or nicardipine. Finally, we used a high dose of amlodipine in the present study. Although this dose of amlodipine (10 mg/kg/day) has been used in other experimental studies (*12*, *28–30*), it did require us to adjust the level of blood pressure reduction among the treatments.

In conclusion, the results of the present study suggest that long-term treatment with amlodipine decreases the generation of reactive oxygen species in several areas of the brain, including the hypothalamus and brainstem. This mechanism might be associated with a reduction in sympathetic nerve activity in SHRSP.

References

1. The ALLHAT Officers and Coordinators for the ALLHAT Collaborative Research Group: Major outcomes in high-risk hypertensive patients randomized to angiotensin-converting enzyme inhibitor or calcium channel blocker *vs* diuretic. The Antihypertensive and Lipid-Lowering Treatment to Prevent Heart Attack Trial (ALLHAT). *JAMA* 2002; **288**: 2981–2997.

2. Julius S, Kjeldsen SE, Weber M, *et al*: Outcomes in hypertensive patients at high cardiovascular risk treated with regimens based on valsartan or amlodipine: the VALUE randomised trial. *Lancet* 2004; **363**: 2022–2031.
3. Furberg CD, Psaty BM, Meyer JV: Nifedipine: dose-related increase in mortality in patients with coronary heart disease. *Circulation* 1995; **92**: 1325–1331.
4. Pahor M, Applegate WB, Williamson JD, *et al*: Health outcomes associated with calcium antagonists compared with other first-line antihypertensive therapies: a meta-analysis of randomized controlled trials. *Lancet* 2000; **356**: 1949–1954.
5. Opie LH, Yasuf S, Küber W: Current status of safety and efficacy of calcium channel blockers in cardiovascular diseases: a critical analysis based on 100 studies. *Prog Cardiovasc Dis* 2000; **43**: 171–196.
6. Chen L, Haught WH, Yang B, Saldeen TG, Parathasarathy S, Mehta JL: Preservation of endogenous antioxidant activity and inhibition of lipid peroxidation as common mechanisms of antiatherosclerotic effects of vitamin E, lovastatin and amlodipine. *J Am Coll Cardiol* 1997; **30**: 569–575.
7. Kataoka C, Egashira K, Ishibashi M, *et al*: Novel anti-inflammatory actions of amlodipine in a rat model of arteriosclerosis induced by long-term inhibition of nitric oxide synthesis. *Am J Physiol Heart Circ Physiol* 2004; **286**: H768–H774.
8. Gerzanich V, Ivanova S, van der Heijden MS, Zhou H, Simard JM: Trans-cellular proliferating cell nuclear antigen gene activation in cerebral vascular smooth muscle by endothelial oxidative injury *in vivo*. *Arterioscler Thromb Vasc Biol* 2003; **23**: 2048–2054.
9. Blezer ELA, Nicolay K, Goldschmeding R, Koomans HA, Joles JA: Reduction of cerebral injury in stroke-prone spontaneously hypertensive rats by amlodipine. *Eur J Pharmacol* 2002; **444**: 75–81.
10. Pitt B, Byington RP, Furberg CD, *et al*, PREVENT Investigators: Effect of amlodipine on the progression of atherosclerosis and the occurrence of clinical events. *Circulation* 2000; **102**: 1503–1510.
11. Zhang X, Hintze TH: Amlodipine releases nitric oxide from canine coronary microvessels: an unexpected mechanism of action of a calcium channel-blocking agent. *Circulation* 1998; **97**: 576–580.
12. Zhou M-S, Jaimes EA, Raij L: Inhibition of oxidative stress and improvement of endothelial function by amlodipine in angiotensin II-infused rats. *Am J Hypertens* 2004; **17**: 167–171.
13. Mason RP, Walter MF, Trumbore MW, Olmstead EG Jr, Mason PE: Membrane antioxidant effects of the charged dihydropyridine calcium antagonist amlodipine. *J Mol Cell Cardiol* 1999; **31**: 275–281.
14. Yamagata K, Ichinose S, Tagami M: Amlodipine and carvedilol prevent cytotoxicity in cortical neurons isolated from stroke-prone spontaneously hypertensive rats. *Hypertens Res* 2004; **27**: 271–282.
15. Binggeli C, Corti R, Sudano I, Luscher TF, Noll G: Effects of chronic calcium channel blockade on sympathetic nerve activity in hypertension. *Hypertension* 2002; **39**: 892–896.
16. Fogari R, Zoppi A, Corradi L, Preti P, Malalamani GD, Mugellini A: Effects of different dihydropyridine calcium antagonists on plasma norepinephrine in essential hypertension. *J Hypertens* 2000; **18**: 1871–1875.
17. Hamada T, Watanabe M, Kaneda T, *et al*: Evaluation of changes in sympathetic nerve activity and heart rate in essential hypertensive patients induced by amlodipine and nifedipine. *J Hypertens* 1998; **16**: 111–118.
18. Ishimitsu T, Kobayashi T, Honda T, *et al*: Protective effects of an angiotensin II receptor blocker and a long-acting calcium channel blocker against cardiovascular organ injuries in hypertensive patients. *Hypertens Res* 2005; **28**: 351–359.
19. Soong TW, Stea A, Hodson CD, Dubel SJ, Vincent SR, Snutch TP: Structure and functional expression of a member of the low voltage-activated calcium channel family. *Science* 1993; **260**: 1133–1136.
20. Miller RJ: Multiple calcium channels and neuronal function. *Science* 1987; **235**: 46–52.
21. Murzenok PP, Huang BS, Leenen FHH: Sympatho-inhibition by central and peripheral infusion of nifedipine in spontaneously hypertensive rats. *Hypertension* 2000; **35**: 631–636.
22. Huang BS, Leenen FHH: Sympathoinhibitory and depressor effects of amlodipine in spontaneously hypertensive rats. *J Cardiovasc Pharmacol* 2003; **42**: 153–160.
23. Kishi T, Hirooka Y, Kimura Y, Ito K, Shimokawa H, Takeshita A: Increased reactive oxygen species in rostral ventrolateral medulla contribute to neural mechanisms of hypertension in stroke-prone spontaneously hypertensive rats. *Circulation* 2004; **109**: 2357–2362.
24. Touyz RM: Reactive oxygen species, vascular oxidative stress, and redox signaling in hypertension. *Hypertension* 2004; **44**: 248–252.
25. Ganafa AA, Walton M, Eatman D, Abukhalaf IK, Bayorh MA: Amlodipine attenuates oxidative stress-induced hypertension. *Am J Hypertens* 2004; **17**: 743–748.
26. De Champlain J, Karas M, Nguyen P, *et al*: Different effects of nifedipine and amlodipine on circulating catecholamine levels in essential hypertensive patients. *J Hypertens* 1998; **16**: 1357–1369.
27. Taddei S, Virdis A, Ghiadoni L, *et al*: Calcium antagonist treatment by lercanidipine prevents hyperpolarization in essential hypertension. *Hypertension* 2003; **41**: 950–955.
28. Yavuz DG, Tugler S, Koçak H, Ozener C, Akoglu E, Akalin S: Angiotensin converting enzyme inhibition and calcium channel blockage improves cyclosporine induced glucose intolerance in rats. *Transplant Proc* 2004; **36**: 171–174.
29. Toblli JE, Stella I, Mazza ON, Fender L, Inserra F: Different effect of losartan and amlodipine on penile structure in male spontaneously hypertensive rats. *Am J Nephrol* 2004; **24**: 614–623.
30. Toba H, Nakagawa Y, Miki S, *et al*: Calcium channel blockades exhibit anti-inflammatory and antioxidative effects by augmentation of endothelial nitric oxide synthase and the inhibition of angiotensin converting enzyme in the N^G-nitro-L-arginine methyl ester-induced hypertensive rat aorta: vasoprotective effects beyond the blood pressure lowering effects of amlodipine and manidipine. *Hypertens Res* 2005; **28**: 689–700.
31. Kishi T, Hirooka Y, Mukai Y, Shimokawa H, Takeshita A: Atorvastatin causes depressor and sympatho-inhibitory

effects with upregulation of nitric oxide synthases in stroke-prone spontaneously hypertensive rats. *J Hypertens* 2003; **21**: 379–386.
32. Ide T, Tsutsui H, Kinugawa S, *et al*: Mitochondrial electron transport complex I is a potential source of oxygen free radicals in the failing myocardium. *Circ Res* 1999; **85**: 357–363.
33. Ide T, Tsutsui H, Kinugawa S, *et al*: Direct evidence for increased hydroxyradicals originating from superoxide in the failing myocardium. *Circ Res* 2000; **86**: 152–157.
34. Ito K, Hirooka Y, Kishi T, *et al*: Rho/Rho-kinase pathway in the brainstem contributes to hypertension caused by chronic nitric oxide synthase inhibition. *Hypertension* 2004; **43**: 156–162.
35. Kimura Y, Hirooka Y, Sagara Y, *et al*: Overexpression of inducible nitric oxide synthase in rostral ventrolateral medulla causes hypertension and sympathoexcitation *via* an increase in oxidative stress. *Circ Res* 2005; **96**: 252–260.
36. Sugawara H, Tobise K, Kikuchi K: Antioxidant effects of calcium antagonists on rat myocardial membrane lipid peroxidation. *Hypertens Res* 1996; **19**: 223–228.
37. Lippoldt A, Kneisel U, Liebner S, *et al*: Structural alterations of tight junctions are associated with loss of polarity in stroke-prone spontaneously hypertensive rat blood–brain barrier endothelial cells. *Brain Res* 2000; **885**: 251–261.
38. Lu C, Chan SL, Mattson MP: The lipid peroxidation product 4-hydroxynoneal facilitates opening of voltage-dependent Ca^{2+} channels in neurons by increasing protein tyrosine phosphorylation. *J Biol Chem* 2002; **277**: 24368–24375.
39. Tseng W-P, Lin-Shiau S-Y: Neuronal death signaling by β-bungarotoxin through the activation of the *N*-methyl-D-aspartate (NMDA) receptor and L-type calcium channel. *Biochem Pharmacol* 2003; **65**: 131–142.
40. Wang R-M, Zhang Q-G, Zhang G-Y: Activation of ERK5 is mediated by *N*-methyl-D-aspartate receptor and L-type voltage-gated calcium channel *via* Src involving oxidative stress after cerebral ischemia in rat hippocampus. *Neurosci Lett* 2004; **357**: 13–16.
41. Fukuo K, Yang J, Yasuda O, *et al*: Nifedipine indirectly upregulates superoxide dismutase expression in endothelial cells *via* vascular smooth muscle cell–dependent pathways. *Circulation* 2002; **106**: 356–361.
42. Napoli C, Salomone S, Godfraind T, *et al*: 1,4-Dihydropyridine calcium channel blockers inhibit plasma and LDL oxidation and formation of oxidation-specific epitopes in the arterial wall and prolong survival in stroke-prone spontaneously hypertensive rats. *Stroke* 1999; **30**: 1907–1915.
43. Hou X, Gobeil F, Marrache AM, *et al*: Increased platelet-activating factor-induced periventricular brain microvascular constriction associated with immaturity. *Am J Physiol Regul Integr Comp Physiol* 2003; **284**: 928–935.
44. Kikugawa K, Kojima T, Yamaki S, Kosugi H: Interpretation of the thiobarbituric acid reactivity of rat liver and brain homogenates in the presence of ferric ion and ethylenediaminetetraacetic acid. *Anal Biochem* 1992; **202**: 249–255.
45. Ohtsuki T, Matsumoto M, Suzuki K, Taniguchi N, Kamada T: Mitochondrial lipid peroxidation and superoxide dismutase in rat hypertensive target organs. *Am J Physiol* 1995; **268**: H1418–H1421.
46. Kishi T, Hirooka Y, Ito K, Sakai K, Shimokawa H, Takeshita A: Cardiovascular effects of overexpression of endothelial nitric oxide synthase in the rostral ventrolateral medulla in stroke-prone spontaneously hypertensive rats. *Hypertension* 2002; **39**: 264–268.
47. Dampney RAL: Functional organization of central pathways regulating the cardiovascular system. *Physiol Rev* 1994; **74**: 323–364.
48. Pilowsky PM, Goodchild AK: Baroreceptor reflex pathways and neurotransmitters: 10 years on. *J Hypertens* 2002; **20**: 1675–1688.
49. Higuchi S, Takeshita A, Ito N, Imaizumi T, Matsuguchi H, Nakamura M: Arterial pressure and heart rate responses to calcium channel blockers administered in the brainstem in rats. *Circ Res* 1985; **57**: 244–251.
50. Zanzinger J: Mechanisms of action of nitric oxide in the brain stem. *Auton Neurosci* 2002; **98**: 24–27.
51. Patel KP, Li Y-F, Hirooka Y: Role of nitric oxide in central sympathetic outflow. *Exp Biol Med* 2001; **226**: 814–824.
52. Hirooka Y, Sakai K, Kishi T, Ito K, Shimokawa H, Takeshita A: Enhanced depressor response to endothelial nitric oxide synthase gene transfer into the nucleus tractus solitarii of spontaneously hypertensive rats. *Hypertens Res* 2003; **26**: 325–331.
53. Berkels R, Taubert D, Bartels H, Bretenbach T, Klaus W, Roesen R: Amlodipine increases endothelial nitric oxide by dual mechanisms. *Pharmacology* 2004; **70**: 39–45.
54. Umemoto S, Tanaka M, Kawahara S, *et al*: Calcium antagonist reduces oxidative stress by upregulating Cu/Zn superoxide dismutase in stroke-prone spontaneously hypertensive rats. *Hypertens Res* 2004; **27**: 877–885.
55. Kerr S, Brosnan J, McIntyre M, Reid JL, Domniczak AF, Hamilton CA: Superoxide anion production is increased in a model of genetic hypertension. *Hypertension* 1999; **33**: 1353–1358.
56. Kimoto-Kinoshita S, Nishida S, Tomura TT: Age-related change of anti-oxidant capacities in the cerebral cortex and hippocampus of stroke-prone spontaneously hypertensive rats. *Neurosci Lett* 1999; **273**: 41–44.
57. Wilson SK: Role of oxygen-derived free radicals in acute angiotensin II-induced hypertensive vascular disease in the rat. *Circ Res* 1990; **66**: 722–734.
58. Zhang XM, Ellis EF: Superoxide dismutase reduces permeability and edema induced by hypertension in rats. *Am J Physiol* 1990; **259**: H497–H503.
59. Grunfeld S, Hamilton CA, Mesaros S, *et al*: Role of superoxide in the depressed nitric oxide production by the endothelium of genetically hypertensive rats. *Hypertension* 1995; **26**: 854–857.
60. Spence JD: Preventing dementia by treating hypertension and preventing stroke. *Hypertension* 2004; **44**: 20–21.
61. Furukawa T, Nukada T, Suzuki K, *et al*: Voltage and pH dependent block of cloned N-type Ca^{2+} channels by amlodipine. *Br J Pharmacol* 1997; **121**: 1136–1140.
62. Uneyama H, Uchida H, Konda T, Yoshimoto R, Akaike N: Selectivity of dihydropyridines for cardiac L-type and sympathetic N-type Ca^{2+} channels. *Eur J Pharmacol* 1999; **373**: 93–100.

Original Article

cAMP-Response Element-Binding Protein Mediates Tumor Necrosis Factor-α-Induced Vascular Cell Adhesion Molecule-1 Expression in Endothelial Cells

Hiroki ONO[1], Toshihiro ICHIKI[1], Hideki OHTSUBO[1], Kae FUKUYAMA[1], Ikuyo IMAYAMA[1], Naoko IINO[1], Satoko MASUDA[1], Yasuko HASHIGUCHI[1], Akira TAKESHITA[1], and Kenji SUNAGAWA[1]

Hypertension causes endothelial dysfunction, which plays an important role in atherogenesis. The vascular cell adhesion molecule-1 (VCAM-1) contributes to atherosclerotic lesion formation by recruiting leukocytes from blood into tissues. Tumor necrosis factor-α (TNFα) induces endothelial dysfunction and VCAM-1 expression in endothelial cells (ECs). We examined whether the cAMP-response element binding protein (CREB), a transcription factor that mediates cytokine expression and vascular remodeling, is involved in TNFα-induced VCAM-1 expression. TNFα induced phosphorylation of CREB with a peak at 15 min of stimulation in a dose-dependent manner in bovine aortic ECs. Pharmacological inhibition of p38 mitogen-activated protein kinase (p38-MAPK) inhibited TNFα-induced CREB phosphorylation. Adenovirus-mediated overexpression of a dominant-negative form of CREB suppressed TNFα-induced VCAM-1 and *c-fos* expression. Although activating protein 1 DNA binding activity was attenuated by overexpression of dominant negative CREB, nuclear factor-κB activity was not affected. Our results suggest that the p38-MAPK/CREB pathway plays a critical role in TNFα-induced VCAM-1 expression in vascular endothelial cells. The p38-MAPK/CREB pathway may be a novel therapeutic target for the treatment of atherosclerosis. (*Hypertens Res* 2006; 29: 39–47)

Key Words: **endothelial factors, cytokine, gene expression, mitogen-activated protein kinase, signal transduction**

Introduction

The initial step of atherogenesis involves attachment of mononuclear leukocytes to endothelial cells (ECs) and migration into the subendothelial space (*1*). Adhesion molecules expressed in ECs play an important role in the attachment of mononuclear leukocytes. Various cardiovascular risk factors including hypertension have been shown to increase the levels of soluble adhesion molecules, such as the vascular cell adhesion molecule-1 (VCAM-1), intercellular adhesion molecule-1 (ICAM-1) and E-selectin (*2–4*). Carotid intima-media thickness has been positively correlated with the plasma level of circulating soluble cellular adhesion molecules (*5*). VCAM-1 is expressed in ECs predisposed to atherosclerotic lesion formation (*6*) and contributes to recruitment of mono-

From the [1]Department of Cardiovascular Medicine, Kyushu University Graduate School of Medical Sciences, Fukuoka, Japan.

This study was supported in part by grants from the Takeda Medical Research Foundation and a Grant-in-Aid for Scientific Research from the Ministry of Education, Culture, Sports, Science and Technology of Japan (14570673).

Address for Reprints: Toshihiro Ichiki, M.D., Department of Cardiovascular Medicine, Kyushu University Graduate School of Medical Sciences, 3–1–1 Maidashi, Higashi-ku, Fukuoka 812–8582, Japan. E-mail: ichiki@cardiol.med.kyushu-u.ac.jp

Received June 16, 2005; Accepted in revised form November 7, 2005.

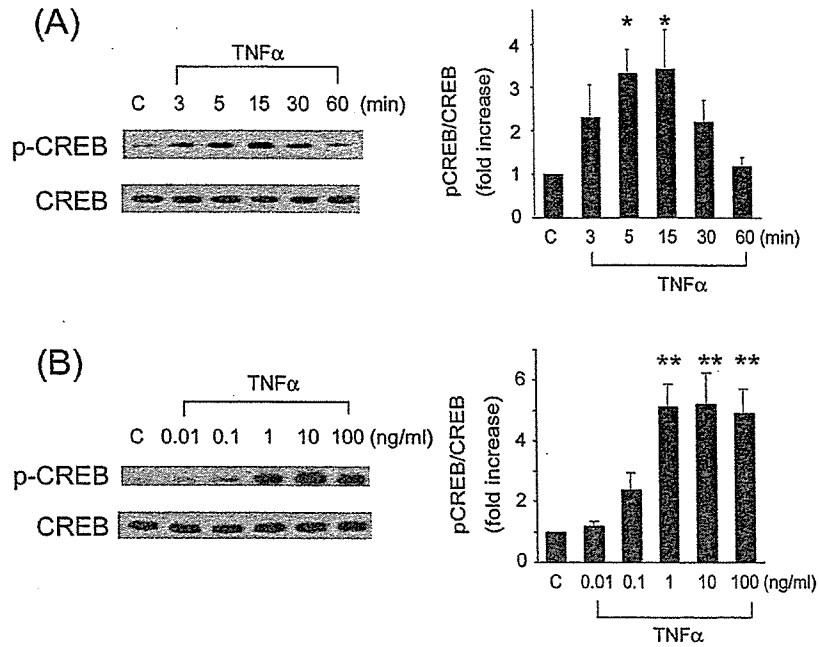

Fig. 1. *CREB is phosphorylated at Ser133 by TNFα. A: Bovine ECs were stimulated with TNFα (1 ng/ml) for varying periods indicated in the figure (n=4). B: Bovine ECs were stimulated with TNFα for 15 min at concentrations varying from 0.01 to 100 ng/ml (n=4). Phosphorylation of CREB was detected by Western blot analysis using a phospho-specific CREB antibody. The density of the specific band was scanned and quantified with an imaging analyzer. The ratio of phosphorylated CREB to total CREB in TNFα-stimulated cells is shown as the relative fold increase compared with that in unstimulated cells. The values are expressed as the mean±SEM.* $^{*}p<0.05$, $^{**}p<0.01$ *vs. the control.*

nuclear leukocytes by binding to α4β1-integrin expressed on leukocytes (*7*).

Tumor necrosis factor-α (TNFα) is a multifunctional cytokine produced by activated macrophages, monocytes and lymphocytes. The vascular EC is an important target of TNFα (*1*, *8*). A previous study demonstrated that *in vivo* blockade of TNFα accelerated functional endothelial recovery after angioplasty (*9*). TNFα is known to modulate the expression of many genes involved in cytoadhesion, thrombosis, and inflammatory response in ECs, resulting in the acquisition of new functional capacities leading to atherosclerosis (*10*). VCAM-1 is one of the molecules induced by TNFα (*11*).

cAMP-response element (CRE)-binding protein (CREB) is a 43 kD nuclear transcription factor belonging to the CREB/ATF family (*12*, *13*). Phosphorylation of the serine residue at 133 (Ser133), which recruits a transcriptional coactivator, CREB-binding protein (CBP) or p300, is necessary for transcriptional activation. The phosphorylation of Ser133 is mediated by a variety of protein kinase pathways, such as 1) protein kinase A (PKA), 2) Ca^{2+}/calmodulin-dependent protein kinase (CaMK) II (*14*), 3) extracellular signal-regulated protein kinase (ERK) (*15*, *16*), 4) p38 mitogen-activated protein kinase (p38-MAPK) (*17*), and 5) phosphatidylinositol 3-kinase (PI3-K) (*18*).

Although TNFα is known to activate transcription factors such as activating protein 1 (AP-1) and nuclear factor-κB (NF-κB) (*19*, *20*), it has not been examined whether TNFα activates CREB in ECs. We investigated whether CREB is activated by TNFα in bovine ECs. We report in the present study that TNFα phosphorylated CREB through p38-MAPK and CREB mediated TNFα-induced VCAM-1 expression.

Methods

Materials

Dulbecco's modified Eagle's medium (DMEM) was purchased from GIBCO BRL (Gaithersburg, USA). Fetal bovine serum (FBS) was purchased from BioWhittaker (Walkersville, USA). Ionomycin, KN93 and SP60125 were purchased from Sigma Chemical Co. (St. Louis, USA). Recombinant human TNFα was a gift from Dainippon Pharmaceutical Co. (Osaka, Japan). PD98059 and wortmannin were purchased from BIOMOL Research Laboratories Inc. (Plymouth Meeting, USA). SB203580 and FR167653, inhibitors of p38-MAPK, were gifts from GlaxoSmithKline and Fujisawa Pharmaceutical Co. (Osaka, Japan), respectively. H89 was purchased from Seikagaku Co. (Tokyo, Japan). Horseradish peroxidase conjugated second antibodies (anti-rabbit or anti-mouse IgG) were purchased from VECTOR Laboratories Inc.

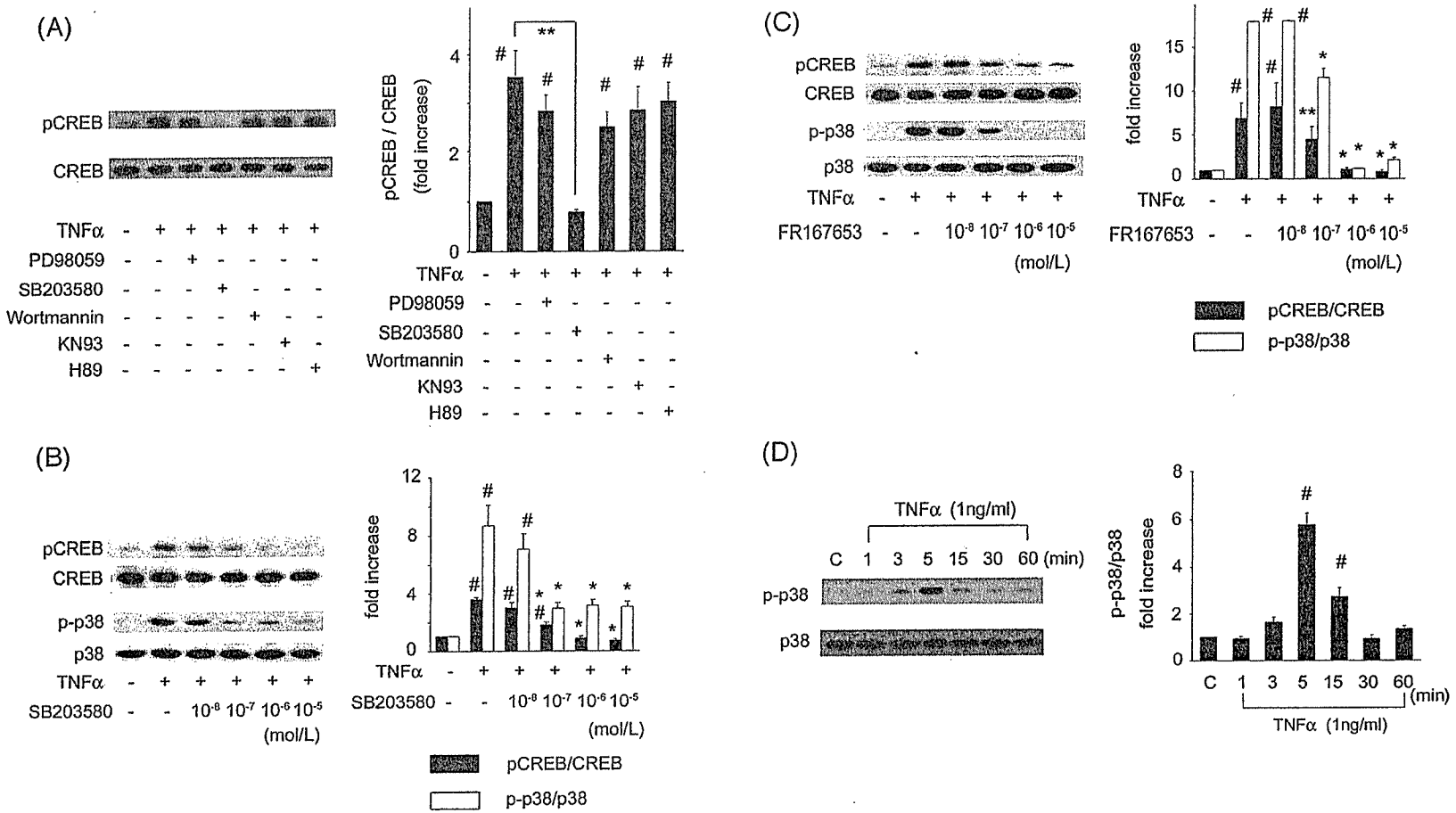

Fig. 2. *The p38-MAPK pathway mediates TNFα-induced CREB phosphorylation. A: Bovine ECs were preincubated with PD98059 (10 μmol/l), SB203580 (10 μmol/l), wortmannin (50 nmol/l), KN93 (10 μmol/l) or H89 (1 μmol/l) for 30 min and stimulated with TNFα (1 ng/ml) for 15 min. Phosphorylation of CREB was detected and analyzed as described in the legend to Fig. 1 (n = 3). The ratio of phosphorylated CREB to total CREB in TNFα-stimulated cells is shown as the relative fold increase compared with that in unstimulated cells. The values are expressed as the mean ± SEM. **p < 0.01 vs. TNFα, #p < 0.01 vs. the control. B, C: Bovine ECs were preincubated with (B) SB203580 or (C) FR167653 at concentrations varying from 10^{-8} to 10^{-5} mol/l for 30 min and stimulated with TNFα (1 ng/ml) for 15 min. D: Bovine ECs were stimulated with TNFα (1 ng/ml) for varying periods indicated in the figure. Phosphorylation of CREB and p38-MAPK was detected and analyzed as described in the legend to Fig. 1 (n = 4–6). The ratio of phosphorylated CREB or p38-MAPK to total CREB or p38-MAPK in TNFα-stimulated cells is shown as the relative fold increase compared with that in unstimulated cells. The values are expressed as the mean ± SEM. #p < 0.01 vs. the control, *p < 0.01, **p < 0.05 vs. TNFα.*

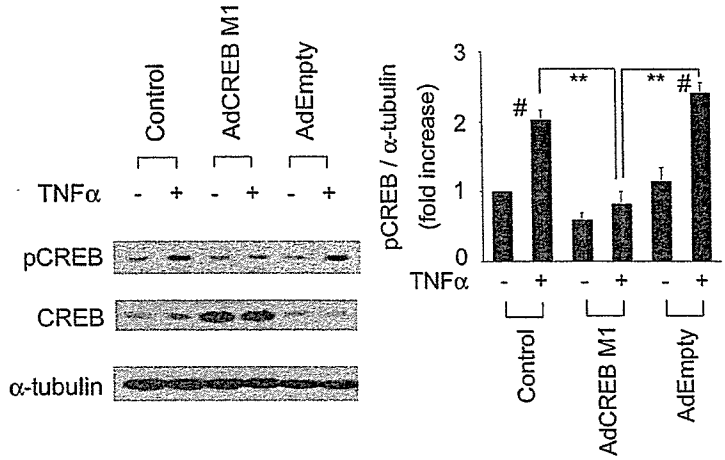

Fig. 3. *AdCREB M1 inhibits TNFα-induced CREB phosphorylation. Bovine ECs were infected with AdCREB M1 (30 MOI) or AdEmpty (30 MOI) and stimulated with or without TNFα (1 ng/ml) for 15 min. TNFα-induced CREB phosphorylation was detected by Western blot analysis (*n = *4). The ratio of phosphorylated CREB to α-tubulin in TNFα-stimulated cells is shown in the right panel as the relative fold increase compared with that in unstimulated cells. The values are expressed as the mean±SEM.* $^{**}p < 0.01$ *vs. AdCREB M1 TNFα (+),* $^{\#}p < 0.01$ *vs. control TNFα (−) or AdEmpty TNFα (−).*

(Burlingame, USA). Other antibodies used in the experiments were obtained from Cell Signaling Technology (Danvers, USA). Other chemical reagents were purchased from Wako Pure Chemicals (Osaka, Japan) unless specifically mentioned.

Cell Culture

The bovine aortic ECs were the gift of Katsuya Hirano (Kyushu University Graduate School of Medical Sciences) and grown in a humidified atmosphere of 95% air/5% CO_2 at 37°C in DMEM with 10% FBS. Passages between 5 and 12 were used for the experiments. The investigation conformed with the Guide for the Care and Laboratory Animals published by the US National Institutes of Health (NIH Publication No. 85-23, revised 1996).

Western Blot Analysis

Bovine ECs were lysed in a sample buffer (5 mmol/l EDTA, 10 mmol/l Tris-HCl, pH 7.6, 1% Triton X-100, 50 mmol/l NaCl, 30 mmol/l sodium phosphate, 50 mmol/l NaF, 1% aprotinin, 0.5% pepstatin A, 2 mmol/l phenylmethylsulfonyl fluoride and 5 mmol/l leupeptin). Western blot analyses of CREB, p38-MAPK and VCAM-1 were performed as described previously (*21*).

Adenovirus Vector Expressing a Dominant Negative Form of CREB

A recombinant adenovirus vector expressing a mutant of CREB (AdCREB M1) (*22*) in which the phosphorylation site at Ser133 was changed to alanine was a gift from Anthony J. Zeleznik (University of Pittsburgh, Pittsburgh, USA). Confluent bovine ECs were washed 2 times with PBS and incubated with AdCREB M1 or adenovirus empty vector (AdEmpty) under gentle agitation for 2 h at room temperature. Then the cells were washed 3 times, cultured in DMEM with 10% FBS for 2 days and used for the experiments. The multiplicity of infection (MOI) value indicates the number of viruses per cell added to a culture dish.

Northern Blot Analysis

Total RNA was prepared according to an acid–guanidinium–thiocyanate–phenol–chloroform extraction method. Northern blot analysis of *c-fos*, VCAM-1 and 18S rRNA was performed as described previously (*21*). The radioactivity of hybridized bands of *c-fos* and VCAM-1 mRNA, and 18S rRNA was quantified with a MacBAS Bioimage Analyzer (Fuji Film Co., Tokyo, Japan).

Preparation of Nuclear Extracts and Gel Mobility Shift Assay

The preparation of nuclear extracts and gel mobility shift assay were performed as described previously (*23*). DNA probes of AP-1 (5′-CGCTTGATGAGTCAGCCGGAA-3′) and NF-κB (5′-AGATGAGGGGACTTTCCCAGGC-3′) were end-labeled with ^{32}P γ-ATP. Ten micrograms of nuclear extracts were incubated with 1×10^5 cpm of labeled DNA probe for 30 min at room temperature and electrophoresed on 4% acrylamide gel. A fifty-fold molar excess of unlabeled DNA was added as a competitor. After electrophoresis, the

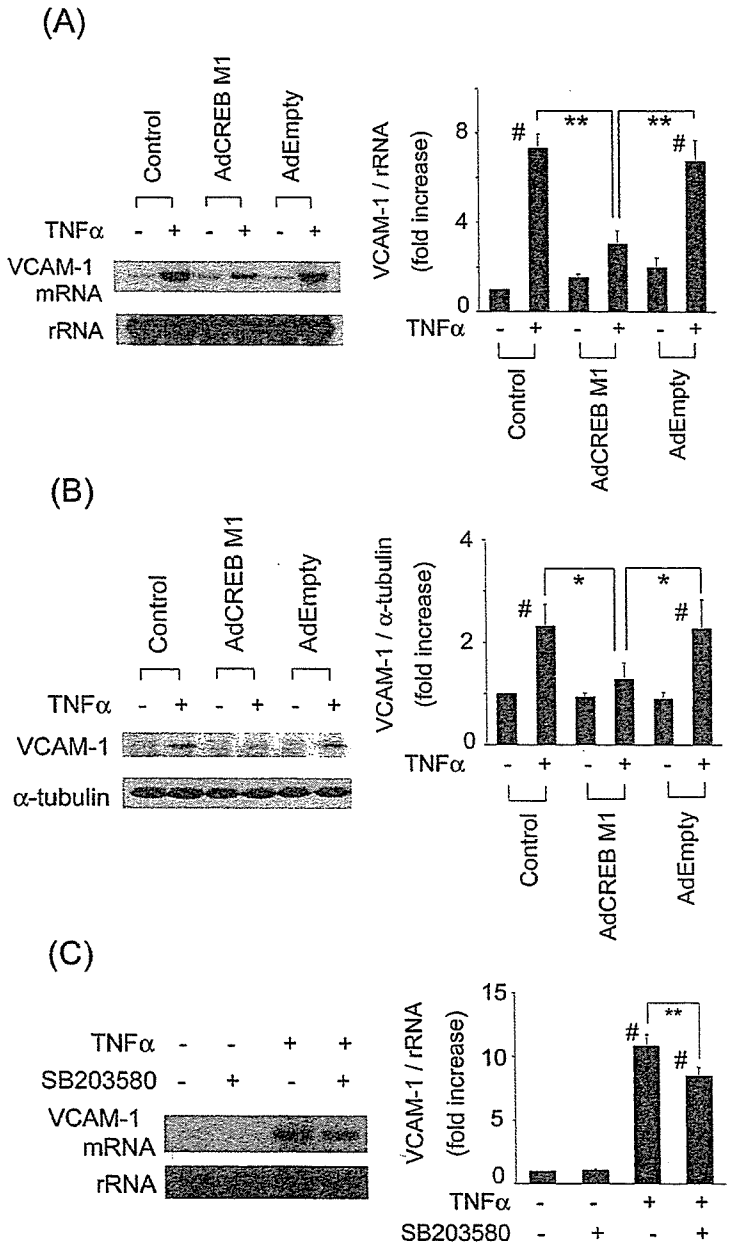

Fig. 4. *AdCREB M1 inhibits TNFα-induced VCAM-1 mRNA and protein expression. A: Bovine ECs were infected with AdCREB M1 (30 MOI) or AdEmpty (30 MOI) and stimulated with or without TNFα (1 ng/ml) for 4 h. TNFα-induced VCAM-1 mRNA expression was detected by Northern blot analysis and the radioactivities of the bands were measured with an imaging analyzer (n = 4). The radioactivity of VCAM-1 mRNA in TNFα-stimulated cells was normalized against that of rRNA and shown as the relative fold increase compared with that in unstimulated cell. B: Bovine ECs were infected with AdCREB M1 (30 MOI) or AdEmpty (30 MOI) and stimulated with or without TNFα (1 ng/ml) for 12 h. TNFα-induced VCAM-1 protein expression was detected by Western blot analysis (n = 4) and the ratio of VCAM-1 expression to α-tubulin in TNFα-stimulated cells is shown in the right panel as the relative fold increase compared with that in unstimulated cells. C: Bovine ECs were preincubated with SB203580 (10 μmol/l) for 30 min and stimulated with TNFα (1 ng/ml) for 4 h. TNFα-induced VCAM-1 mRNA expression was detected by Northern blot. The values are expressed as the mean±SEM.* $^{**}p < 0.01$ vs. *AdCREB M1 TNFα (+) or TNFα,* $^{*}p < 0.05$ vs. *AdCREB M1 TNFα (+),* $^{\#}p < 0.01$ vs. *control TNFα (−) or AdEmpty TNFα (−).*

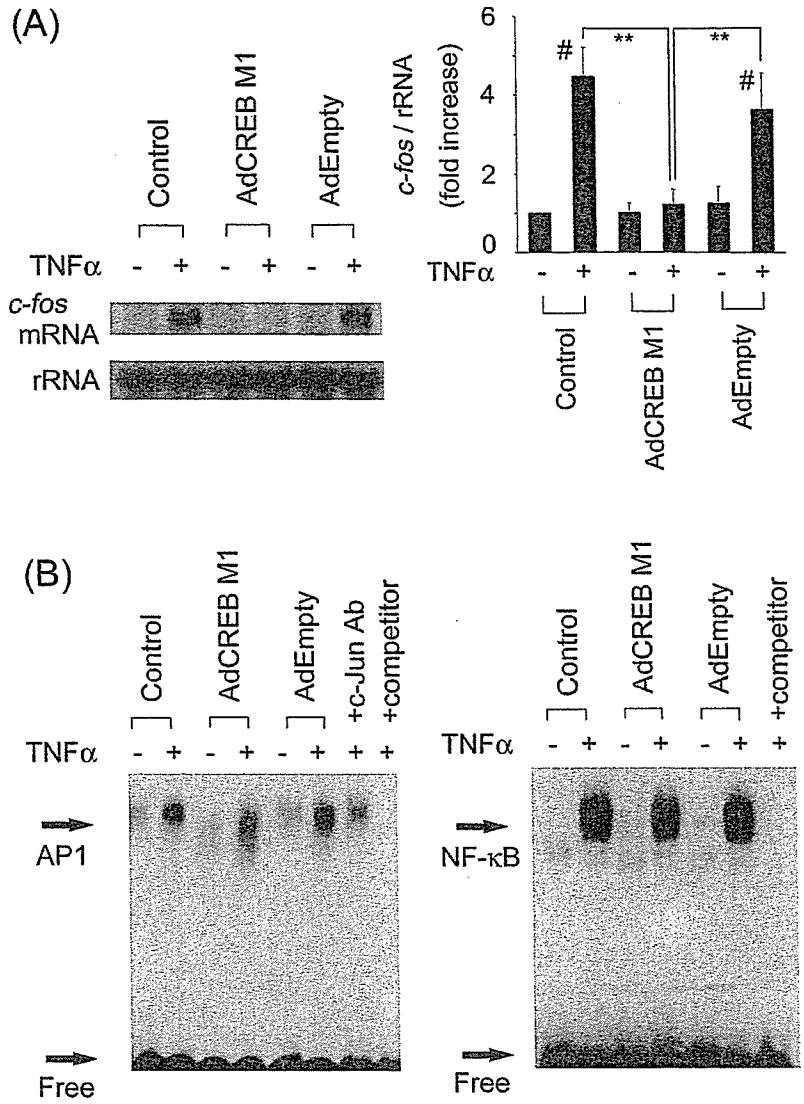

Fig. 5. *AdCREB M1 inhibits TNFα-induced* c-fos *mRNA expression and AP-1 DNA binding activity. A: Bovine ECs were infected with AdCREB M1 (30 MOI) or AdEmpty (30 MOI) and stimulated with or without TNFα (1 ng/ml) for 30 min. TNFα-induced* c-fos *mRNA expression was detected by Northern blot analysis and the radioactivities of the bands were measured with an imaging analyzer* (n=4). *The radioactivity of* c-fos *mRNA was normalized against that of rRNA. The ratio in TNFα-stimulated cells is shown as the relative fold increase compared with that in unstimulated cells. The values are expressed as the mean±SEM.* $^{**}p<0.01$ vs. *AdCREB M1 TNFα (+),* $^{\#}p<0.01$ vs. *control TNFα (−) or AdEmpty TNFα (−). B: Bovine ECs were infected with AdCREB M1 (30 MOI) or AdEmpty (30 MOI) and stimulated with or without TNFα (1 ng/ml) for 4 h. Nuclear extracts were prepared and incubated with radiolabeled AP-1 (left panel) or NF-κB (right panel) probe for 30 min and electrophoresed. A fifty-fold molar excess of unlabeled probe was used as a competitor. For the supershift assay, an antibody against c-Jun was added to the binding reaction mixtures. The same results were obtained in other independent experiments and a representative autoradiogram is shown* (n=4).

gels were dried and exposed to X-ray films.

Statistical Analysis

Statistical analysis was performed with 1-way ANOVA and Fisher's test if appropriate. Values of $p<0.05$ were considered to indicate statistical significance. Data are shown as the mean±SEM.

Results

Phosphorylation of CREB at Ser133 by TNFα

To examine whether CREB is phosphorylated in response to TNFα, we performed Western blot analysis using an antibody that only recognizes the phosphorylated form of CREB at Ser133 (p-CREB). TNFα stimulated phosphorylation of CREB with a peak at 15 min of stimulation (Fig. 1A). TNFα dose-dependently increased phosphorylation of CREB at 15 min of stimulation (Fig. 1B).

The p38-MAPK Pathway Mediates TNFα-Induced CREB Phosphorylation

Several protein kinases are reported to phosphorylate CREB. We examined which pathway is responsible for TNFα-induced CREB phosphorylation. SB203580 (10 μmol/l), a p38-MAPK inhibitor, completely blocked TNFα-induced CREB phosphorylation (Fig. 2A). PD98059 (10 μmol/l), an ERK kinase (MEK) inhibitor, wortmannin (50 nmol/l), an inhibitor of PI3-K, KN93 (10 μmol/l), an inhibitor of CAMKII, and H89 (1 μmol/l), an inhibitor of PKA, did not affect TNFα-induced CREB phosphorylation (Fig. 2A). SP600125, a *c-jun* N-terminal kinase inhibitor, also had no effect on TNFα-induced CREB phosphorylation (data not shown). SB203580 was first described as an inhibitor of p38-MAPK activity that acts by competing with ATP for binding; however, it was later demonstrated that SB203580 also prevents p38-MAPK phosphorylation/activation (*24–26*). SB203580 dose-dependently inhibited TNFα-induced CREB and p38-MAPK phosphorylation (Fig. 2B). To confirm the role of p38-MAPK, we used another p38-MAPK inhibitor, FR167653. FR167653 dose-dependently inhibited TNFα-induced CREB and p38-MAPK phosphorylation (Fig. 2C). TNFα stimulated phosphorylation of p38-MAPK with a peak at 5 min of stimulation, which is faster than phosphorylation of CREB (Fig. 2D). PD98059 and wortmannin at the same concentrations used in Fig. 2 inhibited TNFα-induced ERK and Akt (a target molecule of PI3-K) activation, respectively (data not shown). KN93 and H89 at the same concentrations also inhibited ionomycin- and forskolin-induced CREB phosphorylation, respectively (data not shown). Therefore, the concentrations of these protein kinase inhibitors were sufficient. These data suggest that the p38-MAPK pathway is critical for TNFα-induced CREB phosphorylation.

Overexpression of a Dominant Negative Form of CREB Inhibits TNFα-Induced VCAM-1 Expression

To clarify the role of CREB in the TNFα signaling, we overexpressed a dominant negative form of CREB by an adenovirus vector (AdCREB M1). We used AdEmpty as a negative control for the infection of adenovirus. Phosphorylation of CREB by TNFα was attenuated by infection of AdCREB M1, but not by AdEmpty (Fig. 3). A previous study demonstrated that TNFα stimulated VCAM-1 expression in ECs (*11*). In the present study, AdCREB M1 but not AdEmpty suppressed TNFα-induced VCAM-1 mRNA and protein expression (Fig. 4A, B). SB203580 also suppressed TNFα-induced VCAM-1 mRNA expression (Fig. 4C), suggesting that the p38-MAPK/CREB pathway plays an important role. It is known that TNFα induces VCAM-1 expression through activation of NF-κB and AP-1 (*27*). AP-1 is a heterodimer of c-Fos and c-Jun and CRE is one of the important *cis*-DNA elements regulating *c-fos* gene expression. We therefore hypothesized that dominant negative CREB may affect *c-fos* induction and AP-1 activation. AdCREB M1 but not AdEmpty suppressed TNFα-induced *c-fos* mRNA expression (Fig. 5A). Furthermore, AdCREB M1 suppressed AP-1 DNA binding activity to the consensus sequence induced by TNFα, but it did not affect NF-κB binding activity (Fig. 5B). The binding of AP-1 was specific because the band was eliminated by a 50 mol excess of unlabeled competitor, and the band was supershifted by addition of an antibody against c-Jun. These data suggest that AdCREB M1 may suppress TNFα-induced VCAM-1 gene expression through inhibition of not only CREB but also AP-1 activity.

Discussion

In the present study, we showed that TNFα activated CREB through p38-MAPK. Inhibition of CREB function by a dominant negative molecule suppressed TNFα-induced AP-1 activity and VCAM-1 expression.

The results of a search for *cis*-DNA elements of the VCAM-1 gene promoter by TFSEACH showed the presence of a possible CRE site in the promoter of VCAM-1 at −1686 bp. Therefore, our result suggests that the CRE site of the VCAM-1 gene promoter may play an important role in VCAM-1 expression induced by TNFα. A previous study demonstrated that TNFα stimulated VCAM-1 expression through two NF-κB sites (present at −63 bp and −77 bp from the transcription initiation site) (*11*). Ahmad *et al.* reported that the AP-1/NF-κB complex was induced by TNFα and regulated VCAM-1 gene expression (*27*). AP-1 can interact with other transcription factors and modulate their transcriptional activity (*28*).The p65 subunit of NF-κB requires a co-factor protein for transcriptional activity and can interact with c-Fos and c-Jun through the Rel homology domain (*29*). CRE in the promoter region of the *c-fos* gene plays an important role in the induction of *c-fos* by many stimuli (*30–32*). We confirmed that CRE mediates *c-fos* expression by TNFα. These data suggest that inhibition of AP-1 activity by AdCREB M1 may be involved in the suppression of TNFα-induced VCAM-1 expression. However, further study is necessary to confirm the role of the AP-1 site of the VCAM-1 gene promoter in response to TNFα.

TNFα is known to activate the mitogen-activated protein kinases (MAPKs), such as *c-jun* NH_2-terminal kinase and p38-MAPK in ECs (*33*, *34*). A previous study demonstrated that p38-MAPK mediated actin filament reorganization by several stimuli, such as vascular endothelial growth factor or oxidative stress, in human umbilical vein ECs (*35*). Another study demonstrated that p38-MAPK negatively regulated cell survival and proliferation by FGF-2 stimulation in bovine capillary ECs (*36*). In the present study, we demonstrated that p38-MAPK mediated TNFα-induced CREB phosphorylation and could modulate the expression of cytoadhesion molecules. The p38-MAPK family includes four isoforms, p38α, p38β, p38γ and p38δ. Vascular EC expresses p38α, p38β and p38δ (*37*). SB203580 inhibits p38α and p38β, and thus p38α or p38β may mediate TNFα-induced CREB phosphorylation.

Atherosclerotic lesion progression has been shown to depend on persistent, chronic inflammation in the arterial wall and is characterized by the recruitment of monocytes and lymphocytes to the arterial wall (*38*). Adhesion molecules and chemotactic factors mediate the entry of the leukocytes into the subendothelial space. The first step in adhesion, the rolling of leukocytes along the endothelial surface, is mediated by selectins which bind to carbohydrate ligands on leucocytes (*39*, *40*). The firm adhesion of monocytes and T lymphocytes to endothelium is mediated by VCAM-1 on the endothelium, which interacts with the integrin VLA-4 on monocytes and T lymphocytes (*7*). Therefore, VCAM-1 is assumed to be important for atherosclerogenesis, and knockout strategies have been attempted. Although VCAM-1-null mice die during embryogenesis (*41*), it has been shown that atherosclerotic lesion was reduced that the size of atherosclerotic lesions is reduced in VCAM-1 domain 4-deficient mice (*42*), suggesting that VCAM-1 is indeed an important gene product directly involved in the formation of atherosclerotic lesions.

In the present study, we demonstrated the possible involvement of CREB in TNFα-induced VCAM-1 expression. In addition to TNFα, angiotensin II has been shown to stimulate VCAM-1 expression (*43*, *44*), and we and others previously reported that angiotensin II stimulated phosphorylation of CREB (*32*, *45*). Inhibition of CREB may suppress not only TNFα-induced but also angiotensin II-induced VCAM-1 expression. Furthermore, it was previously reported that high blood pressure activates MAPKs (*46–48*) and that p38-MAPK activation induced by high blood pressure is involved in endothelial dysfunction (*48*). Therefore, inhibition of the p38-MAPK/CREB pathway may attenuate endothelial dysfunction in patients with hypertension. Our data suggest that the p38-MAPK/CREB pathway could be a therapeutic target for the prevention of atherosclerosis.

References

1. Ross R: The pathogenesis of atherosclerosis: a perspective for the 1990s. *Nature* 1993; **362**: 801–809.
2. Blann AD, Tse W, Maxwell SJ, Waite MA: Increased levels of the soluble adhesion molecule E-selectin in essential hypertension. *J Hypertens* 1994; **12**: 925–928.
3. DeSouza CA, Dengel DR, Macko RF, Cox K, Seals DR: Elevated levels of circulating cell adhesion molecules in uncomplicated essential hypertension. *Am J Hypertens* 1997; **10**: 1335–1341.
4. Parissis JT, Venetsanou KF, Mentzikof DG, *et al*: Plasma levels of soluble cellular adhesion molecules in patients with arterial hypertension. Correlations with plasma endothelin-1. *Eur J Intern Med* 2001; **12**: 350–356.
5. Kohara K, Tabara Y, Yamamoto Y, Igase M, Nakura J, Miki T: Genotype-specific association between circulating soluble cellular adhesion molecules and carotid intima-media thickness in community residents: J-SHIPP study. Shimanami Health Promoting Program. *Hypertens Res* 2002; **25**: 31–39.
6. Iiyama K, Hajra L, Iiyama M, *et al*: Patterns of vascular cell adhesion molecule-1 and intercellular adhesion molecule-1 expression in rabbit and mouse atherosclerotic lesions and at sites predisposed to lesion formation. *Circ Res* 1999; **85**: 199–207.
7. Alon R, Kassner PD, Carr MW, Finger EB, Hemler ME, Springer TA: The integrin VLA-4 supports tethering and rolling in flow on VCAM-1. *J Cell Biol* 1995; **128**: 1243–1253.
8. Pober JS, Cotran RS: The role of endothelial cells in inflammation. *Transplantation* 1990; **50**: 537–544.
9. Krasinski K, Spyridopoulos I, Kearney M, Losordo DW: *In vivo* blockade of tumor necrosis factor-alpha accelerates functional endothelial recovery after balloon angioplasty. *Circulation* 2001; **104**: 1754–1756.
10. Berk BC, Abe JI, Min W, Surapisitchat J, Yan C: Endothelial atheroprotective and anti-inflammatory mechanisms. *Ann N Y Acad Sci* 2001; **947**: 93–111.
11. Iademarco MF, McQuillan JJ, Rosen GD, Dean DC: Characterization of the promoter for vascular cell adhesion molecule-1 (VCAM-1). *J Biol Chem* 1992; **267**: 16323–16329.
12. Shaywitz AJ, Greenberg ME: CREB: a stimulus-induced transcription factor activated by a diverse array of extracellular signals. *Annu Rev Biochem* 1999; **68**: 821–861.
13. Mayr B, Montminy M: Transcriptional regulation by the phosphorylation-dependent factor CREB. *Nat Rev Mol Cell Biol* 2001; **2**: 599–609.
14. Sheng M, Thompson MA, Greenberg ME: CREB: a Ca^{2+}-regulated transcription factor phosphorylated by calmodulin-dependent kinases. *Science* 1991; **252**: 1427–1430.
15. Xing J, Ginty DD, Greenberg ME: Coupling of the RAS-MAPK pathway to gene activation by RSK2, a growth factor-regulated CREB kinase. *Science* 1996; **273**: 959–963.
16. Sugawara A, Takeuchi K, Uruno A, Kudo M, Sato K, Ito S: Effects of mitogen-activated protein kinase pathway and co-activator CREP-binding protein on peroxisome proliferator-activated receptor-γ-mediated transcription suppression of angiotensin II type 1 receptor gene. *Hypertens Res* 2003; **26**: 623–628.
17. Tan Y, Rouse J, Zhang A, Cariati S, Cohen P, Comb MJ: FGF and stress regulate CREB and ATF-1 *via* a pathway involving p38 MAP kinase and MAPKAP kinase-2. *EMBO J* 1996; **15**: 4629–4642.

18. Du K, Montminy M: CREB is a regulatory target for the protein kinase Akt/PKB. *J Biol Chem* 1998; **273**: 32377–32379.
19. Baud V, and Karin M: Signal transduction by tumor necrosis factor and its relatives. *Trends Cell Biol* 2001; **11**: 372–377.
20. Chen G, Goeddel DV: TNF-R1 signaling: a beautiful pathway. *Science* 2002; **296**: 1634–1635.
21. Tokunou T, Ichiki T, Takeda K, *et al*: Thrombin induces interleukin-6 expression through the cAMP response element in vascular smooth muscle cells. *Arterioscler Thromb Vasc Biol* 2001; **21**: 1759–1763.
22. Somers JP, DeLoia JA, Zeleznik AJ: Adenovirus-directed expression of a nonphosphorylatable mutant of CREB (cAMP response element-binding protein) adversely affects the survival, but not the differentiation, of rat granulosa cells. *Mol Endocrinol* 1999; **13**: 1364–1372.
23. Funakoshi Y, Ichiki T, Ito K, Takeshita A: Induction of interleukin-6 expression by angiotensin II in rat vascular smooth muscle cells. *Hypertension* 1999; **34**: 118–125.
24. Frantz B, Klatt T, Pang M, *et al*: The activation state of p38 mitogen-activated protein kinase determines the efficiency of ATP competition for pyridinylimidazole inhibitor binding. *Biochemistry* 1998; **37**: 13846–13853.
25. Ryder JW, Fahlman R, Wallberg-Henriksson H, Alessi DR, Krook A, Zierath JR: Effect of contraction on mitogen-activated protein kinase signal transduction in skeletal muscle. Involvement of the mitogen- and stress-activated protein kinase 1. *J Biol Chem* 2000; **275**: 1457–1462.
26. Galan A, Garcia-Bermejo ML, Troyano A, *et al*: Stimulation of p38 mitogen-activated protein kinase is an early regulatory event for the cadmium-induced apoptosis in human promonocytic cells. *J Biol Chem* 2000; **275**: 11418–11424.
27. Ahmad M, Theofanidis P, Medford RM: Role of activating protein-1 in the regulation of the vascular cell adhesion molecule-1 gene expression by tumor necrosis factor-alpha. *J Biol Chem* 1998; **273**: 4616–4621.
28. Chinenov Y, Kerppola TK: Close encounters of many kinds: Fos-Jun interactions that mediate transcription regulatory specificity. *Oncogene* 2001; **20**: 2438–2452.
29. Stein B, Baldwin AS Jr, Ballard DW, Greene WC, Angel P, Herrlich P: Cross-coupling of the NF-kappa B p65 and Fos/Jun transcription factors produces potentiated biological function. *EMBO J* 1993; **12**: 3879–3891.
30. Karin M: The regulation of AP-1 activity by mitogen-activated protein kinases. *J Biol Chem* 1995; **270**: 16483–16486.
31. Ichiki T, Tokunou T, Fukuyama K, Iino N, Masuda S, Takeshita A: Cyclic AMP response element-binding protein mediates reactive oxygen species-induced *c-fos* expression. *Hypertension* 2003; **42**: 177–183.
32. Funakoshi Y, Ichiki T, Takeda K, Tokunou T, Iino N, Takeshita A: Critical role of cAMP-response element-binding protein for angiotensin II-induced hypertrophy of vascular smooth muscle cells. *J Biol Chem* 2002; **277**: 18710–18717.
33. Ichijo H: From receptors to stress-activated MAP kinases. *Oncogene* 1999; **18**: 6087–6093.
34. Kishore R, Luedemann C, Bord E, Goukassian D, Losordo DW: Tumor necrosis factor-mediated E2F1 suppression in endothelial cells: differential requirement of c-Jun N-terminal kinase and p38 mitogen-activated protein kinase signal transduction pathways. *Circ Res* 2003; **93**: 932–940.
35. Rousseau S, Houle F, Landry J, Huot J: p38 MAP kinase activation by vascular endothelial growth factor mediates actin reorganization and cell migration in human endothelial cells. *Oncogene* 1997; **15**: 2169–2177.
36. Matsumoto T, Turesson I, Book M, Gerwins P, Claesson-Welsh L: p38 MAP kinase negatively regulates endothelial cell survival, proliferation, and differentiation in FGF-2-stimulated angiogenesis. *J Cell Biol* 2002; **156**: 149–160.
37. Hale KK, Trollinger D, Rihanek M, Manthey CL: Differential expression and activation of p38 mitogen-activated protein kinase alpha, beta, gamma, and delta in inflammatory cell lineages. *J Immunol* 1999; **162**: 4246–4252.
38. Lusis AJ: Atherosclerosis. *Nature* 2000; **407**: 233–241.
39. Moore KL, Patel KD, Bruehl RE, *et al*: P-selectin glycoprotein ligand-1 mediates rolling of human neutrophils on P-selectin. *J Cell Biol* 1995; **128**: 661–671.
40. Dong ZM, Chapman SM, Brown AA, Frenette PS, Hynes RO, Wagner DD: The combined role of P- and E-selectins in atherosclerosis. *J Clin Invest* 1998; **102**: 145–152.
41. Gurtner GC, Davis V, Li H, McCoy MJ, Sharpe A, Cybulsky MI: Targeted disruption of the murine VCAM1 gene: essential role of VCAM-1 in chorioallantoic fusion and placentation. *Genes Dev* 1995; **9**: 1–14.
42. Cybulsky MI, Iiyama K, Li H, *et al*: A major role for VCAM-1, but not ICAM-1, in early atherosclerosis. *J Clin Invest* 2001; **107**: 1255–1262.
43. Pueyo ME, Gonzalez W, Nicoletti A, Savoie F, Arnal JF, Michel JB: Angiotensin II stimulates endothelial vascular cell adhesion molecule-1 *via* nuclear factor-kappaB activation induced by intracellular oxidative stress. *Arterioscler Thromb Vasc Biol* 2000; **20**: 645–651.
44. Costanzo A, Moretti F, Burgio VL, *et al*: Endothelial activation by angiotensin II through NFkappaB and p38 pathways: involvement of NFkappaB-inducible kinase (NIK), free oxygen radicals, and selective inhibition by aspirin. *J Cell Physiol* 2003; **195**: 402–410.
45. Yoshimoto T, Gochou N, Fukai N, Sugiyama T, Shichiri M, Hirata Y: Adrenomedullin inhibits angiotensin II-induced oxidative stress and gene expression in rat endothelial cells. *Hypertens Res* 2005; **28**: 165–172.
46. Ju H, Behm DJ, Nerurkar S, *et al*: p38 MAPK inhibitors ameliorate target organ damage in hypertension: Part 1. p38 MAPK-dependent endothelial dysfunction and hypertension. *J Pharmacol Exp Ther* 2003; **307**: 932–938.
47. Xu Q, Liu Y, Gorospe M, Udelsman R, Holbrook J: Acute hypertension activates mitogen-activated protein kinases in arterial wall. *J Clin Invest* 1996; **97**: 508–514.
48. Imai G, Satoh T, Kumai T, *et al*: Hypertension accelerates diabetic nephropathy in Wistar fatty rats, a model of type 2 diabetes mellitus, *via* mitogen-activated protein kinase cascades and transforming growth factor-beta1. *Hypertens Res* 2003; **26**: 339–347.

Am J Physiol Heart Circ Physiol 291: H1337–H1344, 2006.
First published April 21, 2006; doi:10.1152/ajpheart.01175.2005.

Blockade of NF-κB improves cardiac function and survival after myocardial infarction

Shunichi Kawano,[1] Toru Kubota,[1] Yoshiya Monden,[1] Takaki Tsutsumi,[1] Takahiro Inoue,[1] Natsumi Kawamura,[1] Hiroyuki Tsutsui,[2] and Kenji Sunagawa[1]

[1]*Department of Cardiovascular Medicine, Kyushu University Graduate School of Medical Sciences, Fukuoka; and*
[2]*Department of Cardiovascular Medicine, Hokkaido University Graduate School of Medicine, Sapporo, Japan*

Submitted 6 November 2005; accepted in final form 12 April 2006

Kawano, Shunichi, Toru Kubota, Yoshiya Monden, Takaki Tsutsumi, Takahiro Inoue, Natsumi Kawamura, Hiroyuki Tsutsui, and Kenji Sunagawa. Blockade of NF-κB improves cardiac function and survival after myocardial infarction. *Am J Physiol Heart Circ Physiol* 291: H1337–H1344, 2006. First published April 21, 2006; doi:10.1152/ajpheart.01175.2005.—NF-κB is a key transcription factor that regulates inflammatory processes. In the present study, we tested the hypothesis that blockade of NF-κB ameliorates cardiac remodeling and failure after myocardial infarction (MI). Knockout mice with targeted disruption of the p50 subunit of NF-κB (KO) were used to block the activation of NF-κB. MI was induced by ligation of the left coronary artery in male KO and age-matched wild-type (WT) mice. NF-κB was activated in noninfarct as well as infarct myocardium in WT + MI mice, while the activity was completely abolished in KO mice. Blockade of NF-κB significantly reduced early ventricular rupture after MI and improved survival by ameliorating congestive heart failure. Echocardiographic and pressure measurements revealed that left ventricular fractional shortening and maximum rate of rise of left ventricular pressure were significantly increased and end-diastolic pressure was significantly decreased in KO + MI mice compared with WT + MI mice. Histological analysis demonstrated significant suppression of myocyte hypertrophy as well as interstitial fibrosis in the noninfarct myocardium of KO + MI mice. Blockade of NF-κB did not ameliorate expression of proinflammatory cytokines in infarct or noninfarct myocardium. In contrast, phosphorylation of c-Jun NH_2-terminal kinase was almost completely abolished in KO + MI mice. The present study demonstrates that targeted disruption of the p50 subunit of NF-κB reduces ventricular rupture as well as improves cardiac function and survival after MI. Blockade of NF-κB might be a new therapeutic strategy to attenuate cardiac remodeling and failure after MI.

cardiac remodeling; inflammation; mitogen-activated protein kinases

NUCLEAR FACTOR-κB (NF-κB) is a key transcription factor that regulates inflammatory processes (1). Recent studies have indicated that NF-κB may play important roles in cardiac hypertrophy and remodeling besides promoting inflammation. First, NF-κB has been shown to be activated in the failing human heart (5, 23), where expression of proinflammatory cytokines is exacerbated (10, 22). Second, in vitro studies have shown that activation of NF-κB is required for hypertrophic growth of cardiomyocytes in response to G protein-coupled receptor agonists, including phenylephrine, endothelin-1, and ANG II (7, 18). Third, recent in vivo studies have demonstrated that blockade of NF-κB ameliorates myocardial hypertrophy in response to aortic banding (12) and chronic infusion of ANG II (9). Finally, blockade of NF-κB improves cardiac function and survival without affecting myocardial inflammation in TNF-α-induced cardiomyopathy (8). Therefore, blockade of NF-κB may be a new therapeutic strategy for heart failure by attenuating myocardial hypertrophy and remodeling.

Myocardial infarction (MI) is a major cause of heart failure in most of the developed countries. NF-κB has been shown to be activated after myocardial ischemia. However, the role of NF-κB in MI remains controversial. Morishita et al. (15) reported that blockade of NF-κB reduced the extent of MI in a rat model of ischemia-reperfusion injury (15), suggesting that activation of NF-κB is cytotoxic in ischemia. The reduction of MI size by NF-κB blockade was also observed in a murine model of ischemia-reperfusion injury (2). In contrast, Misra et al. (14) reported that blockade of NF-κB increased infarct size in a murine model of permanent coronary ligation (14), suggesting that the activation of NF-κB might promote cell survival in MI. Furthermore, no study has investigated the long-term effects of NF-κB blockade on cardiac remodeling and failure late after MI. Therefore, the purpose of the present study was to investigate the role of NF-κB activation in early and late phases of MI using a mouse model of permanent coronary ligation. Mice with targeted disruption of the p50 subunit of NF-κB were used to confer chronic inhibition of NF-κB in vivo (19). The results demonstrated that blockade of NF-κB prevented ventricular rupture early after MI and improved survival by ameliorating cardiac dysfunction in the late phase, suggesting that blockade of NF-κB might be a new therapeutic strategy to attenuate ventricular rupture and remodeling after MI.

MATERIALS AND METHODS

Animal model. Mice with targeted disruption of the p50 subunit of NF-κB (19), backcrossed into the FVB background more than six generations (8, 9), were used to block the activation of NF-κB. These mice were born normally without any major defects. Homoknockout mice (KO) were compared with age- and gender-matched wild-type littermates (WT) in each analysis to minimize the effect of genetic background variation. Male mice at the age of 8–14 wk were used unless mentioned otherwise. We induced MI in both WT and KO mice by ligating the left coronary artery at 2–3 mm from the tip of the left auricle under pentobarbital sodium anesthesia (50 mg/kg ip) as previously reported (20). Sham operation without coronary artery ligation was also performed in WT and KO mice. After the operation, mice were housed under climate-controlled conditions and were provided standard food and water ad libitum. During the study period of 12 wk,

Address for reprint requests and other correspondence: T. Kubota, Dept. of Cardiovascular Medicine, Kyushu Univ. Graduate School of Medical Sciences, 3-1-1 Maidashi, Higashi-ku, Fukuoka 812-8582, Japan (e-mail: kubotat@cardiol.med.kyushu-u.ac.jp).

The costs of publication of this article were defrayed in part by the payment of page charges. The article must therefore be hereby marked "*advertisement*" in accordance with 18 U.S.C. Section 1734 solely to indicate this fact.

cages were inspected daily for animals that had died. All dead mice were examined for the presence of pleural effusion and cardiac rupture as well as MI. The cause of death in each mouse was classified as congestive heart failure when the presence of pleural effusion (serous fluid within the chest wall cavity) and increased lung weight were observed or ventricular rupture when the presence of a blood clot within the pericardial sac was found. This experiment was reviewed and approved by the Committee of the Ethics on Animal Experiment, Kyushu University Graduate School of Medical Sciences and carried out in compliance with the Guideline for Animal Experiment, Kyushu University and the Law (No. 105) and Notification (No. 6) of the Government. The investigation conforms to the *Guide for the Care and Use of Laboratory Animals* published by the National Institutes of Health (NIH Publication No. 85–23, revised 1996).

Electrophoretic mobility shift assay. Activation of NF-κB was evaluated by electrophoretic mobility shift assays (EMSA) according to the manufacturer's instructions (Gel Shift Assay System E3300, Promega, Madison, WI). Nuclear protein was isolated from the myocardium as previously reported (8, 9). For supershift reactions, 1 μl of anti-p50 or -p65 antibody (sc-114X or sc-472X; Santa Cruz, Paso Robles, CA) was added after 20 min of binding reaction, with further incubation for 30 min on ice. Samples were resolved on a 5% acrylamide gel in 0.25% Tris-borate-EDTA buffer.

Echocardiographic and hemodynamic measurements. Four weeks after the operation, mice underwent physiological evaluation with echocardiography and left heart catheterization as previously reported (20). After anesthetization with pentobarbital sodium (30 mg/kg body wt ip, Abbott), a mouse was positioned supine. A 7.5-MHz transducer connected to a dedicated ultrasonographic system (SSD-5500 ALOKA) was applied to the left hemithorax. Two-dimensional targeted M-mode imaging was obtained from the short-axis view at the level of the greatest left ventricular (LV) dimension. After echocardiography, a 1.4-F micromanometer-tipped catheter (Millar Instruments) was inserted into the right carotid artery and then advanced into the LV for pressure measurement under additional anesthesia with 2.5% Avertin (3 μl/g body wt ip, Aldrich Chemical).

Infarct size and myocardial histopathology. After hemodynamic study, the heart was excised and fixed in 4% paraformaldehyde for the evaluation of infarct size and histopathology. Infarct size was determined by methods described previously for rats (17) and also for mice (16, 20). Briefly, the LV was cut from apex to base into four transverse sections. Five-micrometer sections were sliced and stained with Masson's trichrome. Infarct length was measured along the endocardial and epicardial surfaces from each of the LV sections, and the values from all specimens were summed. Total LV circumference was calculated as the sum of endocardial and epicardial segment lengths from all LV sections. Infarct size (in percent) was calculated as total infarct circumference divided by total LV circumference. Cross-sectional area of cardiomyocytes and collagen volume fraction of noninfarct myocardium were determined by quantitative morphometry of tissue sections as previously reported (20).

RNase protection assay. Multiprobe RNase protection assay (RPA) was performed according to the manufacture's protocol (RiboQuant, PharMingen) with 5 μg of total RNA (8, 9). A custom template set containing murine TNF-α; IL-1β; IL-6; transforming growth factor (TGF)-β1; regulated on activation, normal T cell expressed and secreted (RANTES); monocyte chemoattractant protein (MCP)-1; and glyceraldehyde-3-phosphate dehydrogenase (GAPDH) was applied. After RNase digestion, protected probes were resolved on denaturing polyacrylamide gels and quantified by NIH image. The value of each hybridized probe was normalized to that of GAPDH included in each template set as an internal control.

Activity of MAPK. Western blotting analysis was performed by methods described previously (9). Briefly, the noninfarct LV was homogenized with a lysis buffer containing 25 mM Tris, pH 7.4, 150 mM NaCl, 5 mM EDTA, 1 mM Na_3VO_4, 10 mM NaF, 1% (vol/vol) Triton X-100, and 1% (vol/vol) glycerol. Equal amounts of the heart homogenate (30 μg) were separated by SDS-PAGE on 10% (wt/vol) gels, transferred onto a nitrocellulose membrane (Trans-Blot Transfer Medium, Bio-Rad Lab), and blocked with 5% skimmed milk at room temperature for 60 min. The membranes were subjected to immunoblot analyses with anti-phospho-extracellular signal-regulated kinase (ERK) antibody (no. 9106; Cell Signaling Technology), anti-phospho-c-Jun NH_2-terminal kinase (JNK) antibody (no. 9255; Cell Signaling Technology), or anti-phospho-p38 antibody (no. 9211; Cell Signaling Technology). Duplicate samples were subjected to immunoblot analyses with anti-ERK antibody (no. 9102; Cell Signaling Technology), anti-JNK1 antibody (sc-474; Santa Cruz Biotechnology), or anti-p38 antibody (no. 9212; Cell Signaling Technology). Immunodetection was accomplished with a horseradish anti-rabbit or anti-mouse secondary antibody (1:2,000 dilution, Amersham) by using an enhanced chemiluminescence kit (Amersham).

Evaluation of infarct size 24 h after coronary ligation. Evans blue dye (1%) was perfused into the aorta and coronary arteries, and tissue sections were weighed and then incubated with a 1.5% triphenyltetrazolium chloride solution at 37°C for 20 min. The infarct area (pale area), the area at risk (nonblue area), and the total LV area from each section were measured, multiplied by the weight of the section, and then totaled from all sections (20).

DNA ladder. Genomic DNA was isolated from the LV using a proteinase K method as previously described (20). To visualize the DNA laddering, fragmented DNA was amplified by ligation-mediated PCR (Maxim Biotech, South San Francisco, CA). Briefly, after overnight ligation with specially designed adapters, 25 ng of DNA in 50 μl of solution was amplified with 35 cycles of PCR and resolved on a 1.5% agarose/ethidium bromide gel.

Statistics. Results are presented as means ± SD. Survival analysis was performed by the Kaplan-Meier methods. ANOVA with Student-Newman-Keuls post hoc test or χ^2 test was used for statistical comparison. Differences were considered significant at a value of $P < 0.05$.

RESULTS

Activation of NF-κB in infarct and noninfarct myocardium. EMSA was performed with nuclear protein isolated from infarct myocardium 24 h after MI and noninfarct myocardium 7 days after MI. Compared with WT + sham-operated mice, NF-κB was further activated in infarct (Fig. 1*A*) and noninfarct myocardium (Fig. 1*B*) of WT + MI mice. In contrast, activation of NF-κB was completely abolished in KO + sham-operated and KO + MI mice. Most of NF-κB band in infarct myocardium was supershifted with the anti-p50 antibody (Fig. 1*C*), suggesting that the majority of NF-κB was p50-p50 homodimers or p50-p65 heterodimers.

Improved survival after MI in NF-κB KO mice. Within 24 h after the operation, 44 of 119 WT + MI (37%) and 46 of 121 KO + MI mice (38%, $P = 0.973$) died of cardiogenic shock without ventricular rupture or bleeding. In contrast, none of 16 WT + sham-operated and 20 KO + sham-operated mice died after the operation. Survival analysis was performed up to 12 wk in these survived animals. Within 7 days after MI, 25 of 75 WT + MI (33%) and 19 of 75 KO + MI mice (25%, $P = 0.370$) died. Although the total mortality was not different statistically, the rate of ventricular rupture was significantly lower in KO + MI mice (11 of 75) than WT + MI mice (22 of 75, $P < 0.05$). As shown in Fig. 2, the survival rate up to 12 wk after MI was significantly higher in KO + MI mice (73.3%) than WT + MI mice (56.0%, $P < 0.05$). No ventricular rupture was observed after 7 days. All the autopsied mice exhibited marked cardiomegaly and pleural effusion, suggest-

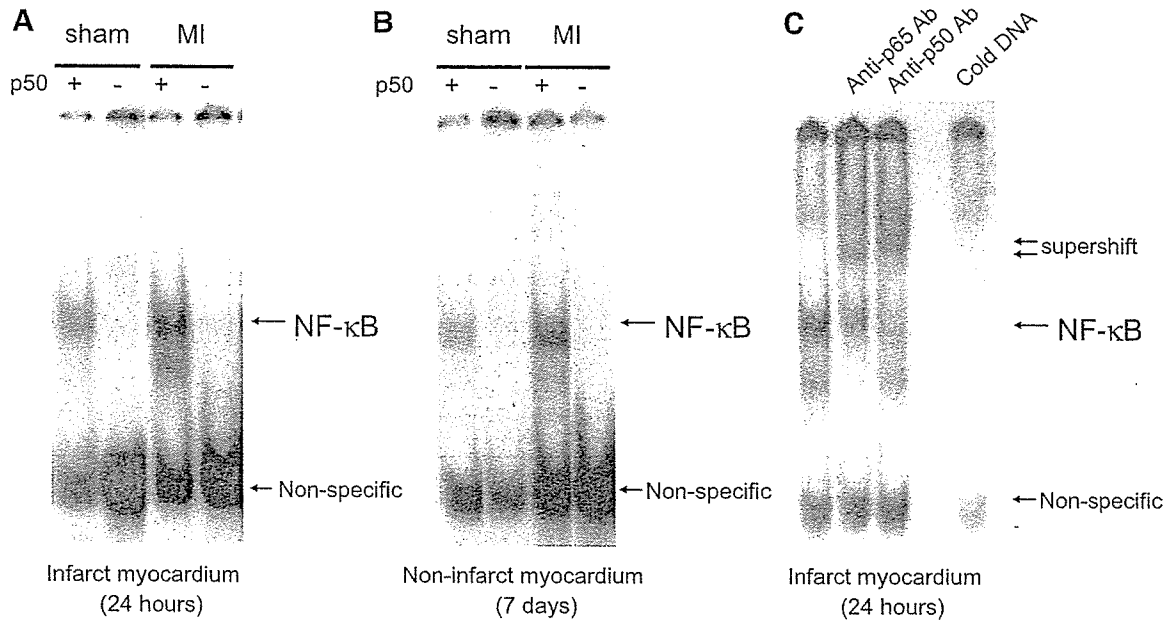

Fig. 1. Electrophoretic mobility shift assay for activated NF-κB after myocardial infarction (MI) in the presence (+) or absence (−) of the p50 subunit. Nuclear proteins were isolated from infarct myocardium 24 h after MI (*A*) and noninfarct myocardium 7 days after MI (*B*). Nuclear proteins were isolated from the corresponding myocardium in sham-operated mice. Supershift analysis was performed by using anti-p50 or -p65 antibody (Ab) to investigate the subunit composition of activated NF-κB in infarct myocardium (*C*).

ing that they died of congestive heart failure. These results suggest that blockade of NF-κB may prevent ventricular rupture early after MI and improve the survival with ameliorating congestive heart failure thereafter.

Attenuated cardiac dysfunction in KO + MI mice. Cardiac function was evaluated 4 wk after the operation by using echocardiography and left heart catheterization. The results are summarized in Table 1. Echocardiography revealed no significant differences in cardiac morphology and function between WT + sham-operated and KO + sham-operated mice. Although both WT + MI and KO + MI mice had significantly larger LV dimensions and significantly lower fractional shortening than WT + sham-operated mice, LV systolic dimension was significantly smaller and fractional shortening was significantly higher in KO + MI mice than in WT + MI mice.

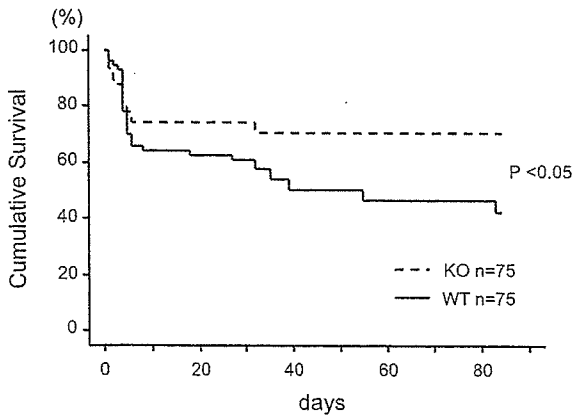

Fig. 2. Kaplan-Meier survival curves of wild-type (WT) and NF-κB knockout mice (KO) after MI.

As in echocardiographic parameters, LV pressure parameters were not significantly different between WT + sham-operated and KO + sham-operated mice. LV systolic pressure, maximum rate of rise of LV pressure ($+dP/dt_{max}$), and peak rate of LV pressure fall ($-dP/dt_{min}$) were significantly lower and LV end-diastolic pressure was significantly higher in WT + MI mice than in WT + sham-operated mice. In contrast, there were no significant differences in LV systolic pressure, $+dP/dt_{max}$, $-dP/dt_{min}$, and end-diastolic pressure between KO + sham-operated and KO + MI mice. LV systolic pressure and $+dP/dt_{max}$ were significantly higher and LV end-diastolic pressure was significantly lower in KO + MI mice than WT + MI mice. These results suggest that LV dysfunction after MI was significantly ameliorated in KO mice.

Infarct size was evaluated after hemodynamic evaluation in each mouse. Because infarct size was not different between WT + MI and KO + MI mice (Table 1), the differences in cardiac function were not attributable to infarct size variation.

Amelioration of myocyte hypertrophy and interstitial fibrosis in KO + MI mice. Table 2 summarizes the heart and lung weights 4 wk after the operation. Compared with WT + sham-operated mice, there were significant increases in LV weight, atrial weight, and lung weight in WT + MI mice, consistent with the increased LV end-diastolic pressure after MI. No differences in RV weight, LV weight, atrial weight, and lung weight were observed between WT + sham-operated and KO + sham-operated mice. Compared with WT + MI mice, there were significant decreases in atrial weight and lung weight in KO + MI mice, in agreement with the attenuated elevation of LV end-diastolic pressure in KO + MI mice.

Cross-sectional area of cardiomyocytes and collagen volume fraction of noninfarct myocardium were evaluated with Masson-trichrome staining (Fig. 3*A*). As summarized in Fig. 3*B*,

Table 1. *Left ventricular function and infarct size*

	WT + Sham Operated	KO + Sham Operated	WT + MI	KO + MI
n	6	6	12	13
Echocardiographic data				
Heart rate, beats/min	464±49	467±58	444±58	444±48
End-diastolic dimension, mm	3.38±0.31	3.20±0.30	5.09±0.50*	4.91±0.48*
End-systolic dimension, mm	1.80±0.36	1.62±0.19	4.30±0.57*	3.86±0.46*†
Fractional shortening, %	46.7±5.9	49.0±1.7	15.8±3.8*	21.7±3.7*†
Infarct wall thickness, mm	NA	NA	0.41±0.07	0.48±0.08
Noninfarct wall thickness, mm	0.97±0.16	0.97±0.10	1.14±0.18	1.08±0.08
Hemodynamic data				
Heart rate, beats/min	414±21	399±35	407±28	417±30
Systolic pressure, mmHg	94.8±5.3	95.7±7.0	86.0±9.0*	96.2±9.6†
End-diastolic pressure, mmHg	1.8±2.1	2.1±1.9	7.9±4.9*	4.5±4.6†
$+dP/dt_{max}$, mmHg/s	9,655±2,403	9,655±742	6,562±1,516*	8,231±1,844†
$-dP/dt_{min}$, mmHg/s	5,485±799	4,660±736	3,814±865*	4,378±875*
Infarct size, %	NA	NA	44.9±6.1	45.3±6.9

Data are means ± SD; *n* indicates no. of animals studied. NA, not applicable. KO, NF-κB knockout; $+dP/dt_{max}$, maximum rate of rise of left ventricular pressure; $-dP/dt_{min}$, peak rate of left ventricular pressure fall. *$P < 0.05$ vs. wild type (WT) + sham operated; †$P < 0.05$ vs. WT + myocardial infarction (MI).

the cross-sectional area of cardiomyocytes in noninfarct myocardium was significantly increased in WT + MI mice. In contrast, the cross-sectional area was not increased statistically in KO + MI mice. As summarized in Fig. 3*C*, collagen volume fraction was significantly increased in WT + MI mice compared with WT + sham-operated mice and was smaller in KO + MI mice. These results indicated that myocyte hypertrophy and interstitial fibrosis in noninfarct myocardium after MI were attenuated in KO mice.

Myocardial expression of cytokines. Expression of proinflammatory cytokines was assessed by multiprobe RPA (Fig. 4). Proinflammatory cytokines and chemokines, including RANTES, TNF-α, IL-1β, IL-6, TGF-β, and MCP-1, were upregulated in infarct myocardium 24 h after MI in KO mice as well as in WT mice (Fig. 4, *A* and *B*). Although we had expected that the expression of proinflammatory cytokines and chemokines would be attenuated by NF-κB KO, there were no differences in the expression of IL-1β, IL-6, TGF-β, and MCP-1 between WT + MI and KO + MI mice. On the contrary, the expression of RANTES and TNF-α was enhanced in KO + MI mice.

As in the infarct myocardium, expression of proinflammatory cytokines was evaluated in noninfarct myocardium 4 wk after MI (Fig. 4, *C* and *D*). Compared with WT + sham-operated mice, expression of TNF-α and IL-6 was significantly increased in the noninfarct myocardium of WT + MI mice. Blockade of NF-κB activation did not affect IL-6 but rather enhanced TNF-α expression in KO + MI mice. These results suggest that the induction of proinflammatory cytokines in infarct and noninfarct myocardium was mediated by NF-κB-independent pathways.

Phosphorylation of MAP kinases. Activation of MAP kinases has been shown to play an important role in cardiac hypertrophy and remodeling. As shown in Fig. 5, both ERK and JNK, but not p38, were phosphorylated in noninfarct myocardium 7 days after MI in WT mice. There were no significant differences in the protein levels of ERK, JNK, or p38 between WT and KO mice. However, NF-κB KO almost completely abolished the phosphorylation of JNK, although it did not affect that of ERK. The selective abrogation of JNK phosphorylation might play an important role in the attenuation of cardiac remodeling and dysfunction after MI in KO mice.

Infarct size and apoptosis 24 h after MI. Because the rate of ventricular rupture was significantly lower in KO + MI mice, another group of animals with WT + MI ($n = 5$) and KO + MI ($n = 6$) were evaluated at 24 h after MI to elucidate the underlying mechanisms. As summarized in Table 3, the infarct area in KO + MI mice was significantly lower than that in WT + MI mice, which may suggest less myocardial damage early after MI in KO mice. As indicated by the DNA ladder assay, although apoptosis was increased in the infarct myocardium at 24 h after MI, the extent of apoptosis was not different between WT and KO mice (Fig. 6). Therefore, the difference in infarct size may not be attributed to apoptosis.

Table 2. *Heart and lung weights*

	WT + Sham Operated	KO + Sham Operated	WT + MI	KO + MI
n	6	6	13	13
BW, g	30.7±1.5	30.6±2.5	29.9±1.7	30.0±1.9
Heart weight/BW, mg/g	4.31±0.71	4.28±0.49	5.71±0.75*	4.99±0.49*†
Left ventricular weight/BW, mg/g	2.89±0.49	2.80±0.28	3.64±0.64*	3.23±0.42
Right ventricular weight/BW, mg/g	0.75±0.18	0.85±0.20	0.76±0.25	0.78±0.12
Atrial weight/BW, mg/g	0.68±0.23	0.63±0.24	1.30±0.37*	0.97±0.28
Lung weight/BW, mg/g	4.91±0.55	5.02±0.77	6.62±1.37*	5.05±0.62†

Data are means ± SD; *n* indicates no. of animals studied; BW, body weight. *$P < 0.05$ vs. WT + sham operated; †$P < 0.05$ vs. WT + MI.